NASA TECHNICAL NOTE

NASA TN D-8302

NASA TN D-8302

RADIATION FROM A CURRENT FILAMENT DRIVEN BY A TRAVELING WAVE

D. M. Le Vine and Robert Meneghini

Goddard Space Flight Center
Greenbelt, Md. 20771

NATIONAL AERONAUTICS AND SPACE ADMINISTRATION • WASHINGTON, D. C. • OCTOBER 1976

1. Report No.	2. Government Accession No.	3. Recipient's Catalog No.
NASA TN D-8302		

4. Title and Subtitle

Radiation from a Current Filament Driven by a Traveling Wave

5. Report Date: October 1976

6. Performing Organization Code: 953

7. Author(s): D. M. Le Vine and Robert Meneghini

8. Performing Organization Report No.: G-76115

9. Performing Organization Name and Address

Goddard Space Flight Center
Greenbelt, Maryland 20771

10. Work Unit No.: 175-10-40

11. Contract or Grant No.

12. Sponsoring Agency Name and Address

National Aeronautics and Space Administration
Washington, D. C. 20546

13. Type of Report and Period Covered: Technical Note

14. Sponsoring Agency Code

15. Supplementary Notes

16. Abstract

Solutions are presented for the electromagnetic fields radiated by an arbitrarily oriented current filament located above a perfectly conducting ground plane and excited by a traveling current wave. Both an approximate solution, valid in the fraunhofer region of the filament and predicting the radiation terms in the fields, and an exact solution, which predicts both near and far field components of the electromagnetic fields, are presented. Both solutions apply to current waveforms which propagate along the channel but are valid regardless of the actual waveshape. The exact solution is valid only for waves which propagate at the speed of light, and the approximate solution is formulated for arbitrary velocity of propagation.

The spectrum—magnitude of the Fourier transform—of the radiated fields is computed by assuming a compound exponential model for the current waveform. The effects of channel orientation and length, as well as velocity of propagation of the current waveform and location of the observer, are discussed. It is shown that both velocity of propagation and an effective channel length, $L(1 - \cos \phi)$, where L is the actual channel length and ϕ is the angle between the filament and the line from filament to observer, are important in determining the shape of the spectrum.

17. Key Words (Selected by Author(s))	18. Distribution Statement
Radiation from filament lightning spectra	Unclassified—Unlimited Cat. 33

19. Security Classif. (of this report)	20. Security Classif. (of this page)	21. No. of Pages	22. Price*
Unclassified	Unclassified	68	$4.25

For sale by the National Technical Information Service, Springfield, Virginia 22161

All measurement values are expressed in the International System of Units (SI) in accordance with NASA Policy Directive 2220.4, paragraph 4.

CONTENTS

RADIATION FROM A CURRENT FILAMENT DRIVEN BY A TRAVELING WAVE

D. M. Le Vine and Robert Meneghini
Goddard Space Flight Center
Greenbelt, Maryland

INTRODUCTION

This document presents a solution for the electric field radiated from an arbitrarily oriented current filament located above a perfectly conducting plane and driven by a traveling current wave. Both an exact and an approximate solution are obtained. The approximate solution is obtained by simplifying the integrand in expressions for the magnetic vector potential in a conventional manner (i.e., the "far-field" approximation) and, as a result, yields only the radiation terms of the electric field measured by an observer in the fraunhofer region of the filament. On the other hand, a closed-form expression for the fields can be obtained without resorting to approximation in the special case in which the current wave propagates along the filament at the speed of light in the medium surrounding the filament. This "exact" solution predicts both radiation and near (e.g., induction) fields and applies regardless of the distance of the observer from the filament, length of the filament, or frequency. Both solutions apply regardless of the current waveform: the only restriction on the current waveform required in the approximate solution is that it be a propagating wave, and the only additional restriction on the current waveform required for the "exact" solution is that the wave propagate with the speed of light in the medium in which the filament resides.

This problem arose during a study of radiation from lightning. The signal radiated by a lightning flash (called an "atmospheric" or just "sferic") is important as a noise source in the design of communications systems and is also as a diagnostic in the study of lightning itself. It may also be possible to relate the radio-frequency radiations from lightning to meteorological observables of the parent storm cell: for example, it has been suggested (References 1, 2, and 3) that a high frequency of occurrence of lightning is related to the existence of tornadoes.

The physical nature of lightning permits analysis at radio frequencies, in terms of a piecewise linear model of radiating electrical elements. For example, a typical cloud-to-ground lightning event begins as a series of ionizing steps (stepped leader) along which current propagates to establish a conducting channel between the charge in the cloud and the ground. The leader process is followed by a large current surge (the return stroke) which exchanges charge between the cloud and the ground. The current in the return stroke propagates along the channel at

velocities approaching the speed of light (Reference 4), and the shape of the current wave is roughly exponential (Appendix A).

An obvious natural beginning point for the calculation of the fields radiated by a piecewise linear model is to use the "far-field" approximation to calculate the fields radiated by each current element in the model. Unfortunately, questions of validity arise when this approximation is used for lightning, because interest often lies in relatively low-frequency behavior (the peak energy radiated by a return stroke is centered near 10 kHz) and because the lightning channel is often long enough (on the order of a few kilometers) so that being in the far field cannot be guaranteed even at relatively large distances from the flash. On the other hand, an exact solution exists for this problem whenever the propagating current wave travels at the speed of light in the medium surrounding the current element. Although not precisely appropriate to lightning because of the restriction on the velocity of propagation, this solution is close enough to reality to provide insight into the near-field and low-frequency behavior of the field electromagnetic fields; it also provides a standard with which to assess the applicability of the far-field approximation.

The purpose of this document is to present both the exact and the far-field solutions for representing radiation from lightning and to use these solutions to illustrate the effect of various channel parameters on the spectra (i.e., magnitude of the Fourier transform) of the fields radiated from lightning. The following section presents the exact solution for both the electric and magnetic fields radiated from a current filament driven by a traveling wave of arbitrary shape. The next section presents the equivalent solution, obtained by making far-field approximations, and the following section compares the two solutions. This comparison indicates that the approximate solution fails at low frequencies in a regime which may be of interest in lightning studies. The comparison is followed by examples of the effect of filament orientation, velocity of propagation, filament length, and the observer's orientation on the spectra observed from a typical return stroke. Finally, a model is presented for a transfer function for the radiation process.

EXACT SOLUTION

Consider a current filament, $\bar{J}(\bar{r}, t)$, above a perfectly conducting plane (the z = 0 plane) as shown in figure 1. Assume that $\bar{J}(\bar{r}, t)$ has the form:

$$\bar{J}(\bar{r}, t) = \hat{\ell}\, f\left(t - \frac{\hat{\ell} \cdot \bar{r}}{c}\right) \tag{1}$$

where $\hat{\ell}$ is a unit vector parallel to the filament, and in the direction of current flow, $\bar{r}$ is the position vector of a point on the filament, and c = 3 x 10^8 m/s is the speed of light. Thus, $\bar{J}(\bar{r},t)$ is a current pulse with shape f(t) which propagates in the $\hat{\ell}$ direction at the speed of light.

A solution for the Fourier transform,* $\tilde{\bar{E}}(\bar{r}, \nu)$, of the radiated electric field, $\bar{E}(\bar{r},t)$, is to be obtained here by Fourier transforming Maxwell's equations (with respect to time) and then solving the transformed equations. This, in turn, is done most conveniently in terms of a

*The superscript "tilda" denotes a Fourier transform. For example: $\tilde{g}(\nu) = \int_{-\infty}^{\infty} g(t) \exp(j2\pi\nu t)\, dt$.

magnetic vector potential, $\tilde{\bar{A}}(\bar{r}, \nu)$. By noting that $\tilde{\bar{J}}(\bar{r}, \nu) = \hat{\ell}\,\tilde{f}(\nu)\exp(jk\,\hat{\ell} \cdot r)$ where $k = 2\pi\nu/c$ and employing the image theorem for currents, the following result is obtained for the i^{th} (rectangular) component of the magnetic vector potential:

$$\tilde{A}_i(\bar{r}, \nu) = \mu \ell_i \int \tilde{f}(\nu)\, e^{jk\,\hat{\ell} \cdot \bar{r}'} \left[\frac{e^{jkR}}{4\pi R} - \epsilon_i \frac{e^{jkR_I}}{4\pi R_I}\right] d\bar{r}' \qquad (2)$$

where the integration is over the filament and where

$$R = |\bar{r}_0 - \bar{r}'| = \sqrt{(x_0 - x')^2 + (y_0 - y')^2 + (z_0 - z')^2} \qquad (3a)$$

$$R_I = |\bar{r}_0 - \bar{r}'_I| = \sqrt{(x - x')^2 + (y - y')^2 + (z + z')^2} \qquad (3b)$$

$$\epsilon_i = \begin{cases} +1 & \text{if } i = x \text{ or } y \qquad (3c) \\ -1 & \text{if } i = z \qquad (3d) \end{cases}$$

$\bar{r}_0$ = the position vector of the observer

By transforming to a coordinate system in which one axis is parallel to the filament, equation 2 can be reduced to a single integral. Let this axis be the z-axis, and denote coordinates of the observer and filament expressed in the new system by $\bar{r}'$ and $\bar{r}''$, respectively:

$$\tilde{A}_i(\bar{r}'_0, \nu) = \mu \ell_i \tilde{f}(\nu) \int_a^b e^{jkz''} \left[\frac{e^{jkr}}{4\pi r} - \epsilon_i \frac{e^{jkr_I}}{4\pi r_I}\right] dz'' \qquad (4)$$

where

$$r = \sqrt{(x'_0 - x''_s)^2 + (y'_0 - y''_s)^2 + (z'_0 - z'')^2} \qquad (5a)$$

$$r_I = \sqrt{\rho^2 + 4\,[\,z'_0 \cos\phi - x'_0 \sin\phi\,]\,[\,z'' \cos\phi - x''_s \sin\phi\,]} \qquad (5b)$$

and where x_s'' and y_s'' are the x- and y-coordinates, respectively, of the filament as seen in the rotated reference frame. The rotation was accomplished by first rotating counterclockwise about the z-axis through the angle θ until the x-axis lay in the plane formed by $\hat{\ell}$ and the z-axis, and then rotating counterclockwise about the new y-axis through the angle ϕ until the z-axis was parallel to $\hat{\ell}$. (See Appendix B.)

Now, in the first integral in equation 4 (i.e., the integral over the source terms), make the change of variables:

$$U = r + (z'' - z_0') \tag{6a}$$

and in the second integral let

$$U_I = r_I + [(z'' - z_0') + 2(z_0' \cos^2 \phi - x_0' \sin \phi \cos \phi)] \tag{6b}$$

This results in the following:

$$\tilde{A}_i(\bar{r}_0', \nu) = \mu \ell_i \tilde{f}(\nu) \left\{ e^{jkz_0'} \int_{U(a)}^{U(b)} \frac{e^{jku}}{4\pi u} du - \right. \tag{7}$$

$$\left. - \epsilon_i \exp\left[jk(-z_0' + 2\sin\phi(z_0' \sin\phi + x_0' \cos\phi))\right] \int_{U_I(a)}^{U_I(b)} \frac{e^{jku_I}}{4\pi u_I} du_I \right\}$$

By transforming back to the original reference frame (Appendix B), and noting that

$$\sum_{i=1}^{3} \ell_i \epsilon_i \hat{\chi}_i = \hat{\ell}'$$

where $\hat{\ell}' = \hat{\ell} - 2(\hat{\ell} \cdot \hat{z})\hat{z}$ is a unit vector in the direction opposite to the image current, the following vector form is obtained for the magnetic vector potential:

$$\tilde{\bar{A}}(r_0, \nu) = \mu \tilde{f}(\nu) \left\{ \hat{\ell} e^{jk\hat{\ell}} \cdot \bar{r}_0 \int_{U(a)}^{U(b)} \frac{e^{jku}}{4\pi u} du \right.$$

$$\left. - \hat{\ell}' e^{jk\hat{\ell}'} \cdot \bar{r}_0 \int_{U'(a)}^{U'(b)} \frac{e^{jku'}}{4\pi u'} du' \right\} \tag{8}$$

where for i = a, b:

$$U(i) = |\bar{\rho}_i| - \hat{\ell} \cdot \bar{\rho}_i \tag{9a}$$

$$U'(i) = |\bar{\rho}'_i| - \hat{\ell}' \cdot \bar{\rho}'_i \tag{9b}$$

and

$$\bar{\rho}_i = \bar{r}_0 - \bar{r}_i \tag{9c}$$

$$\bar{\rho}'_i = \bar{r}_0 - \bar{r}'_i \tag{9d}$$

where $\bar{r}_a$ and $\bar{r}_b$ are the position vectors of the end points of the current filament, $\bar{r}_o$ is the position vector of the observer, and $\bar{r}'_a = \bar{r}_a - 2(\bar{r}_a \cdot \hat{z})\hat{z}$ and $\bar{r}'_b = \bar{r}_b - 2(\bar{r}_b \cdot \hat{z})\hat{z}$ are the position vectors of the end points of the image current filament.

The electric-field intensity, $\tilde{\bar{E}}(\bar{r}_o, \nu)$, can be computed from equation 8 by means of the formula:

$$\tilde{\bar{E}}(\bar{r}_o, \nu) = jkc \left[\tilde{\bar{A}}(\bar{r}_o, \nu) + \frac{1}{k^2} \nabla (\bar{\nabla} \cdot \tilde{\bar{A}}) \right] \tag{10}$$

The procedure is relatively straightforward and can eventually be written in the following form:

$$\tilde{\bar{E}}(\bar{r}_o, \nu) = \sqrt{\mu/\epsilon}\, \tilde{f}(\nu) \left\{ \left[\frac{e^{jk\rho_b}}{4\pi\rho_b} \bar{\epsilon}(\rho_b) - \frac{e^{jk\rho_a}}{4\pi\rho_a} \bar{\epsilon}(\rho_a) \right] - \right.$$

$$\left. - \left[\frac{e^{jk\rho'_b}}{4\pi\rho'_b} \bar{\epsilon}'(\rho'_b) - \frac{e^{jk\rho'_a}}{4\pi\rho'_a} \bar{\epsilon}'(\rho'_a) \right] \right\} \tag{11}$$

where for i = a,b:

$$\bar{\epsilon}(\rho_i) = e^{jk\hat{\ell}\cdot\bar{r}_i}\left[\sqrt{\frac{1+\hat{\ell}\cdot\nabla\rho_i}{1-\hat{\ell}\cdot\nabla\rho_i}}\;\hat{\epsilon}(\rho_i) + j\frac{\nabla\rho_i}{k\rho_i}\right] \tag{12a}$$

$$\bar{\epsilon}'(\rho_i') = e^{jk\hat{\ell}'\cdot\bar{r}_i'}\left[\sqrt{\frac{1+\hat{\ell}'\cdot\nabla\rho_i'}{1-\hat{\ell}'\cdot\nabla\rho_i'}}\;\hat{\epsilon}'(\rho_i') + j\frac{\nabla\rho_i'}{k\rho_i'}\right] \tag{12b}$$

$$\hat{\epsilon}(\rho_i) = \frac{\hat{\ell} - (\hat{\ell}\cdot\nabla\rho_i)\nabla\rho_i}{\sqrt{1-(\hat{\ell}\cdot\nabla\rho_i)^2}} \tag{12c}$$

$$\hat{\epsilon}'(\rho_i') = \frac{\hat{\ell}' - (\hat{\ell}'\cdot\nabla\rho_i')\nabla\rho_i'}{\sqrt{1-(\hat{\ell}'\cdot\nabla\rho_i')^2}} \tag{12d}$$

$$\rho_i = \sqrt{(x_o-x_i)^2+(y_o-y_i)^2+(z_o-z_i)^2} = |\bar{r}_o - \bar{r}_i| \tag{12e}$$

$$\rho_i' = \sqrt{(x_o-x_i)^2+(y_o-y_i)^2+(z_o+z_i)^2} = |\bar{r}_o - \bar{r}_i'| \tag{12f}$$

Note that vectors $\hat{\epsilon}(\rho_i)$ and $\hat{\epsilon}(\rho_i')$ are unit vectors in the direction of the radiation component of electric field associated with the source and image current, respectively. Note, also, that the solution contains four terms, each of which involves the coordinates of the observer and one of the end points of the source or image filament. The two terms associated with $\hat{\epsilon}(\rho_i)$ involve the end points of the source, and the two terms associated with $\hat{\epsilon}(\rho_i')$ involve the end points of the image. Consequently, the radiation from the filament can be treated as if it were emanating from the end points of the source and image filament only.

In the solution for $\tilde{\tilde{E}}(\bar{r}_o,\nu)$, note the presence of the terms that are dependent on $\nabla\rho_i/k\rho_i$. These terms represent inductive (i.e., nonradiation) components of the electric-field intensity and become negligible in the limit of large $k\rho_i$.

The magnetic-field intensity associated with the current filament can also be obtained from equation 10 by means of the formula:

$$\tilde{\tilde{H}}(\bar{r}_o,\nu) = \frac{1}{\mu}\,\bar{\nabla}\times\tilde{\tilde{A}}(\bar{r}_o,\nu) \tag{13}$$

The calculation is again straightforward, although somewhat lengthy, and may be simplified with the aid of the vector identities:

$$\bar{\nabla} \times (\hat{\ell}\,\phi) = \nabla\phi \times \hat{\ell} + \phi\bar{\nabla} \times \hat{\ell} \tag{14a}$$

$$\nabla(\phi\,\theta) = \phi\,\nabla\theta + \theta\,\nabla\phi \tag{14b}$$

Note that, for i = a,b, $\nabla U(i) = \nabla\rho_i - \hat{\ell}$ and similarly that, in the case of the image, $\nabla U'(i) = \nabla\rho_i' - \hat{\ell}'$; thus:

$$\tilde{\bar{H}}(\bar{r}_o, \nu) = \tilde{f}(\nu)\left\{\left[\frac{e^{jk\rho_b}}{4\pi\rho_b}\ \bar{h}(\rho_b) - \frac{e^{jk\rho_a}}{4\pi\rho_a}\ \bar{h}(\rho_a)\right] - \left[\frac{e^{jk\rho_b'}}{4\pi\rho_b'}\ \bar{h}'(\rho_b') - \frac{e^{jk\rho_a'}}{4\pi\rho_a'}\ \bar{h}'(\rho_a')\right]\right\} \tag{15}$$

where for i = a,b:

$$\bar{h}(\rho_i) = e^{jk\hat{\ell}\cdot\bar{r}_i}\sqrt{\frac{1 + \hat{\ell}\cdot\nabla\rho_i}{1 - \hat{\ell}\cdot\nabla\rho_i}}\ \hat{h}(\rho_i) \tag{16a}$$

$$\bar{h}'(\rho_i') = e^{jk\hat{\ell}\cdot\bar{r}_i'}\sqrt{\frac{1 + \hat{\ell}'\cdot\nabla\rho_i'}{1 - \hat{\ell}'\cdot\nabla\rho_i'}}\ \hat{h}'(\rho_i') \tag{16b}$$

$$\hat{h}(\rho_i) = \frac{\nabla\rho_i \times \hat{\ell}}{\sqrt{1 - (\hat{\ell}\cdot\nabla\rho_i)^2}} \tag{16c}$$

$$\hat{h}'(\rho_i') = \frac{\nabla\rho_i' \times \hat{\ell}'}{\sqrt{1 - (\hat{\ell}'\cdot\nabla\rho_i')^2}} \tag{16d}$$

The unit vectors $\hat{h}(\rho_i)$ and $\hat{h}'(\rho_i')$ are in the direction of the magnetic-field intensity associated with the source and image current filament, respectively.

Note that the solution for the magnetic intensity does not contain terms which depend on powers of $1/k\rho_i$ higher than the first. Also, the electric and magnetic fields associated with each end point (i.e., those attributable to one of the four terms in the solution) are orthogonal,

and the fields associated with the source filament only or the image filament only are orthogonal, but the total electric and magnetic fields are orthogonal only in the special case in which the image and source are coplanar. That is, in the absence of boundaries, the total radiation fields from a single source are orthogonal, but the boundary, acting as an effective second source, can result in nonorthogonal electric and magnetic fields, even in the far field.

Finally, the magnitude of the radiation components of the electric and magnetic fields associated with a given end point are proportional, the proportionality constant being the characteristic impedance of the medium, $\sqrt{\mu/\epsilon}$. As previously stated, these fields are also orthogonal. Therefore, in some respects, the fields associated with each end point behave as if there were a small current source located at the end point.

APPROXIMATE SOLUTION

A solution is presented here for the problem treated above, radiation from a current filament driven by a traveling wave and located above a conducting plane, by employing the far-field approximations; that is, assuming that the observer is far enough from the current filament that $k\rho >> 1$ and $kL^2/\rho << 1$, where L is the length of the filament and ρ is the distance from the filament to the observer. When this approximation is made, the restriction to currents which travel at the speed of light, c, is no longer necessary and the following current waveform which propagates with speed v in the $\hat{\ell}$ direction can be treated:

$$\bar{J}(\bar{r}, t) = \hat{\ell} f\left(t - \frac{\hat{\ell} \cdot \bar{r}}{v}\right) \tag{17}$$

Other than this minor change, the solution is formulated initially as in the preceeding section. Thus, the magnetic vector potential is:

$$\tilde{\bar{A}}(\bar{r}_o, \nu) = \mu \tilde{f}(\nu) \int_{\text{filament}} e^{j2\pi\nu\left[\frac{\hat{\ell} \cdot \bar{r}'}{v}\right]} \left[\frac{e^{jkR}}{4\pi R} \hat{\ell} - \frac{e^{jkR_I}}{4\pi R_I} \hat{\ell}'\right] d\bar{r}' \tag{18}$$

where all quantities are as defined in equation 3.

The electric field is obtained from the preceeding equation by means of equation 10, and noting that $\nabla[\bar{\nabla} \cdot (\hat{\ell}\phi)] = (\hat{\ell} \cdot \bar{\nabla})\nabla\phi$ for the constant vector ℓ, the following result is obtained:

$$\tilde{\bar{E}}(\bar{r}_o, \nu) = jk\sqrt{\mu/\epsilon}\ \tilde{f}(\nu) \int_{\text{filament}} e^{j2\pi\nu\left[\frac{\ell \cdot \hat{r}'}{v}\right]} \left\{ \left[\hat{\ell} + \frac{1}{k^2} (\hat{\ell} \cdot \bar{\nabla}) \nabla \right] \frac{e^{jkR}}{4\pi R} - \right.$$

$$\left. - \left[\hat{\ell}' + \frac{1}{k^2} (\hat{\ell}' \cdot \bar{\nabla}) \nabla \right] \frac{e^{jkR_I}}{4\pi R_I} \right\} d\bar{r}' \qquad (19)$$

To evaluate the integrals in equation 19, assume that the distance from the filament to the observer is larger than the length of the filament and expand R and R_I in a power series about the center of the filament. Thus, in the case of the source filament,

$$\begin{aligned} R &= |\bar{r}_o - \bar{r}'| = |(\bar{r}_o - \bar{r}_c) + (\bar{r}_c - \bar{r}')| \\ &= \sqrt{|\bar{r}_o - \bar{r}_c|^2 + |\bar{r}_c - \bar{r}'|^2 + 2(\bar{r}_o - \bar{r}_c) \cdot (\bar{r}_c - \bar{r}')} \\ &\simeq |\bar{r}_o - \bar{r}_c| + |\bar{r}_c - \bar{r}'| \cos\phi + \frac{1}{2} \left[\frac{|\bar{r}_c - \bar{r}'|^2}{|\bar{r}_o - \bar{r}_c|} \right] \end{aligned} \qquad (20)$$

where

$$\cos\phi = \frac{(\bar{r}_o - \bar{r}_c) \cdot (\bar{r}_c - \bar{r}')}{|\bar{r}_o - \bar{r}_c|\ |\bar{r}_c - \bar{r}'|} \qquad (21)$$

and where $\bar{r}_c$ is the position vector of the filament center. Now, let $\rho_c = |\bar{r}_o - \bar{r}_c|$, and assume that

$$kL^2/\rho_c << 1 \qquad (22a)$$

$$kL >> 1 \qquad (22b)$$

where L is the length of the filament. Then, $R \cong \rho_c + |\bar{r}_c - \bar{r}'| \cos\phi$ for use in the exponential, and $R \cong \rho_c$ elsewhere. Repeating this argument for the image distance R_I and substituting the results into equation 19, it follows that:

$$\tilde{\bar{E}}(\bar{r}_o, \nu) = jk\sqrt{\mu/\epsilon}\ \ \tilde{f}(\nu)\ \left\{\left[\hat{\ell} + \frac{1}{k^2}\ (\hat{\ell}\cdot\bar{\nabla})\nabla\right]\ \frac{e^{jk\rho_c}}{4\pi\rho_c}\ \ I(\nu) - \right.$$

$$\left. - \left[\hat{\ell}' + \frac{1}{k^2}\ (\hat{\ell}'\cdot\bar{\nabla})\nabla\right]\frac{e^{jk\rho_c'}}{4\pi\rho_c'}\ \ I'(\nu)\right\} \tag{23}$$

where:

$$I(\nu) = \int_{\text{filament}} e^{j2\pi\nu\left[\frac{\hat{\ell}\cdot\bar{r}'}{v}\right]}\ e^{j2\pi\rho\left[\frac{|\bar{r}_c - \bar{r}'|}{c}\ \cos\phi\right]}\ d\bar{r}' \tag{24a}$$

$$I'(\nu) = \int_{\text{filament}} e^{j2\pi\nu\left[\frac{\ell'\cdot r'}{v}\right]}\ e^{j2\pi\nu\left[\frac{|r_c' - r_I'|}{c}\ \cos\phi'\right]}\ dr' \tag{24b}$$

The vectors associated with the image filament are:

$$\bar{r}_c' = \bar{r}_c - 2(\bar{r}_c\cdot\hat{z})\hat{z} \tag{25a}$$

$$\bar{r}_I' = \bar{r}' - 2(\bar{r}'\cdot\hat{z})\hat{z} \tag{25b}$$

$$\rho_c' = |\bar{r}_o - \bar{r}_c'| \tag{25c}$$

To evaluate integrals $I(\nu)$ and $I'(\nu)$, rotate to a coordinate system in which the filament is parallel to the z-axis as in the preceeding section and as described in Appendix B, and then perform the z-integration in a coordinate system with z-origin at the filament center. Note that, in this coordinate system, $|\bar{r}_c - \bar{r}'|\cos\varphi = (z_c - z'')\,\hat{\ell}\cdot\nabla\rho_c$; therefore

$$I(\nu) = \int_a^b e^{j2\pi\nu} \left[\frac{z''}{v}\right] e^{-j2\pi\nu/c\left[(z'' - z_c)\,\hat{\ell}\,\cdot\,\nabla\rho_c\right]}\, dz''$$

$$= e^{jk\eta z_c} \int_{-L/2}^{L/2} e^{jk\,[\eta - \hat{\ell}\,\cdot\,\nabla\rho_c]\,z''}\, dz'' \qquad (26a)$$

$$= e^{jk\eta z_c} \left\{ L\ \mathrm{sinc}\ [\ \tfrac{1}{2}\,kL\,(\eta - \hat{\ell}\,\cdot\,\nabla\rho_c)\ ] \right\}$$

where $\eta = c/\nu$. Similarly, in the case of the image,

$$I'(\nu) = e^{jk\eta z_c'} \left\{ L\ \mathrm{sinc}\ [\ \tfrac{1}{2}\,kL\,(\eta - \hat{\ell}'\,\cdot\,\nabla\rho_c')\ ] \right\} \qquad (26b)$$

On transforming back to the original reference frame, replace z_c and z_c' by $z_c = \hat{\ell}\cdot\bar{r}_c$ and $z_c' = \hat{\ell}'\cdot\bar{r}_c'$.

The remaining vector operations are straightforward and yield the following results:

$$\left[\hat{\ell} + \frac{1}{k^2}\,(\hat{\ell}\,\cdot\,\bar{\nabla})\,\nabla\right] \frac{e^{jk\rho_c}}{4\pi\rho_c} = \left\{ \hat{\ell}\left[1 + \frac{(\hat{\ell}\,\cdot\,\nabla\rho_c)\nabla\rho_c}{k\rho_c}\right] - \right.$$

$$\left. - \left[1 + j\,\frac{3}{k\rho_c} - \frac{3}{(k\rho_c)^2}\right]\ (\hat{\ell}\,\cdot\,\nabla\rho_c)\nabla\rho_c \right\} \frac{e^{jk\rho_c}}{4\pi\rho_c} \qquad (27a)$$

$$\left[\hat{\ell}' + \frac{1}{k^2}\ (\hat{\ell}'\,\cdot\,\bar{\nabla})\,\nabla\right] \frac{e^{jk\rho_c'}}{4\pi\rho_c'} = \left\{ \hat{\ell}'\left[1 + \frac{(\hat{\ell}'\,\cdot\,\nabla\rho_c')\ \rho_c'}{k\rho_c'}\right] - \right.$$

$$\left. - \left[1 + j\,\frac{3}{k\rho_c'} - \frac{3}{(k\rho_c')^2}\right]\ (\hat{\ell}'\,\cdot\,\nabla\rho_c')\nabla\rho_c' \right\} \frac{e^{jk\rho_c'}}{4\pi\rho_c'} \qquad (27b)$$

Now, keeping only terms of lowest order in $k\rho_c$, the following results for electric field are obtained:

$$\tilde{\bar{\bar{E}}}(\bar{r}_o, \nu) = \sqrt{\mu/\epsilon}\ \tilde{f}(\nu) \left\{ [\hat{\ell} - (\hat{\ell} \cdot \nabla\rho_c)\nabla\rho_c] \frac{e^{jk\rho_c}}{4\pi\rho_c} I(\nu) - [\hat{\ell}' - (\hat{\ell}' \cdot \nabla\rho_c')\nabla\rho_c'] \frac{e^{jk\rho_c'}}{4\pi\rho_c'} I'(\nu) \right\} \tag{28}$$

where

$$I(\nu) = jkLe^{+jk\eta(\hat{\ell} \cdot \bar{r}_c)} \operatorname{sinc}[\tfrac{1}{2} kL(\eta - \hat{\ell} \cdot \nabla\rho_c)] \tag{29a}$$

$$I'(\nu) = jkLe^{+jk\eta(\hat{\ell}' \cdot \bar{r}_c')} \operatorname{sinc}[\tfrac{1}{2} kL(\eta - \hat{\ell}' \cdot \nabla\rho_c')] \tag{29b}$$

The magnetic field intensity can be obtained from equation 13 in a straightforward manner. After making the far-field approximations and keeping only lowest order terms in $k\rho_c$, the following form results:

$$\tilde{\bar{\bar{H}}}(\bar{r}_o, \nu) = f(\nu) \left\{ (\nabla\rho_c \times \hat{\ell}) \frac{e^{jk\rho_c}}{4\pi\rho_c} I(\nu) - (\nabla\rho_c' \times \hat{\ell}') \frac{e^{jk\rho_c'}}{4\pi\rho_c'} I'(\nu) \right\} \tag{30}$$

The solution in equation 30 is valid for the arbitrary index of refraction, η; however, in the special case, $\eta = 1$, which is the assumption used above in the treatment of the "Exact Solution," the far-field solution can be put into a form even more similar to that obtained for the complete solution. Adopting the notation used in the preceeding section, the following forms are obtained for the far-field solutions when $\eta = 1$:

$$\tilde{\bar{\bar{E}}}(\bar{r}_o, \nu) = 2j\sqrt{\mu/\epsilon}\ \tilde{f}(\nu) \left\{ \frac{e^{jk\rho_c}}{4\pi\rho_c} \bar{\epsilon}_R(\rho_c) \sin[\tfrac{1}{2} kL(1 - \hat{\ell} \cdot \nabla\rho_c)] - \frac{e^{jk\rho_c'}}{4\pi\rho_c'} \bar{\epsilon}_R'(\rho_c') \sin[\tfrac{1}{2} kL(1 - \hat{\ell}' \cdot \nabla\rho_c')] \right\} \tag{31a}$$

$$\tilde{\bar{H}}(\bar{r}_o, \nu) = 2j\tilde{f}(\nu) \left\{ \frac{e^{jk\rho_c}}{4\pi\rho_c} \bar{h}(\rho_c) \sin\left[\tfrac{1}{2} kL\left(1 - \hat{\ell} \cdot \nabla\rho_c\right)\right] - \right. \tag{31b}$$

$$\left. - \frac{e^{jk\rho'_c}}{4\pi\rho'_c} \bar{h}'(\rho'_c) \sin\left[\tfrac{1}{2} kL\left(1 - \hat{\ell}' \cdot \nabla\rho'_c\right)\right] \right\}$$

where all quantities are as previously defined except that $\bar{\epsilon}_R(\rho_c)$ and $\bar{\epsilon}'_R(\rho'_c)$ are the vector components of equations 12a and 12b associated with $\hat{\epsilon}(\rho)$ and $\hat{\epsilon}'(\rho')$, respectively; that is, associated with the radiation terms only.

Equations 31a and 31b obviously have a form similar to the radiation component of the complete solution, except that, whereas the complete solution (equations 11 and 15) gave the appearance that the radiation came from the ends of the filament, the far-field solution appears to emanate from the filament center and, in comparison with the complete solution, is weighted by a spatial "transfer function," $2j \sin[\tfrac{1}{2}kL(1 - \hat{\ell} \cdot \nabla\rho)]$, associated with the filament.

COMPARISON OF EXACT AND APPROXIMATE SOLUTIONS

The solution presented in "Exact Solution" is exact in the sense that no mathematical approximations were needed to obtain a solution in closed form. For this reason, this solution provides a useful standard with which to compare the approximate solution obtained above. Comparison of the two solutions yields insight into the usefulness of the far-field approximation and the nature of its shortcomings.

As a first point, note that making the far-field approximation in the exact solution (equations 11 and 15) yields a result identical to the approximate (far-field approximation) solution obtained above (equations 31a and 31b). The details are given in Appendix C. In making the far-field approximation in the exact solution, the approximations must be made after the integrations over the filament have been performed, whereas, in deriving the approximate solutions (as in "Approximate Solution"), the same approximations are made before performing the integrations. Appendix C shows that the end result is the same, giving credence to the approximate solution.

The conditions imposed by the far-field approximations used to obtain the approximate solution are that, in addition to $L/\rho \ll 1$, $k\rho \gg 1$ and $kL^2/\rho \ll 1$ which would suggest, for fixed ρ and L, a frequency band in which the approximate solution faithfully represents the true solution. Certainly, as $k\rho$ becomes smaller, the nonradiation terms in the exact solution become significant, and the approximate solution, which contains only radiation fields, must fail. Appendix D contains a more quantitative assessment for an observer located on the surface. It shows that, at low frequencies, as expected, the far-field solution fails to agree with the exact solution whenever the nonradiation terms become significant. The exact solution is actually singular in $k\rho$, but the far-field solution is not. However, the solutions do not agree at low frequencies even when only radiation terms are compared.

Appendix D shows that the power spectrum for the radiation terms of the electric field as predicted by the exact solution becomes a constant times the spectrum of the current waveform, $| f(\nu) |$ as $k \to 0$, whereas the far-field approximation is proportional to k times $| \tilde{f}(\nu) |$ as $k \to 0$, so that even the radiation terms exhibit a different low-frequency behavior.

The relative low-frequency behavior of the exact and far-field solutions is illustrated in figures 2 through 6 for a current waveform with exponential shape. (A three-exponential model is used for the current. This waveform is shown in figures 7 and 8 and is discussed in Appendix A. The spectrum, $| \tilde{f}(\nu) |$, associated with this waveform is constant at low frequencies and decreases as $1/\nu$ for large frequencies.) In each of figures 2 through 6, 20 times the logarithm (base 10) of the magnitude of the electric field is plotted along the ordinate, and frequency is plotted along the abscissa. In figures 2 through 4, the observer is located on the surface at increasing distance (5, 50, and 500 km, respectively) from the origin. The current element is a vertical filament 1.5 km long with one end at the origin (i.e., on the surface). Each figure shows three curves, which represent the exact solution, the far-field (approximate) solution, and the radiation component only of the exact solution. Because of the nonradiation terms, the exact solution appears as $| \tilde{f}(\nu) |/k$ near $k = 0$. Because $| \tilde{f}(\nu) |$ is a constant for $k = 0$ for the exponential waveform, this solution is singular at zero frequency. This singularity is evident in each figure where, for low enough frequency, the exact solution begins to increase with decreasing frequency. The asymptote for this low-frequency behavior is a straight line with (negative) slope of 20 dB/decade. On the other hand, the radiation component of the exact solution approaches a constant times $| \tilde{f}(\nu) |$ for small ν, as is evident in each of the three figures. The low-frequency behavior of the approximate solution is different from both of these asymptotes: it decreases as $1/\nu$ for low frequency. The effect of increasing the distance from the observer to the source is both to decrease the magnitude of the spectrum at a given frequency and to shift toward lower frequency the point at which the three curves—exact, radiation, and approximate solutions—begin to differ. This is because the criterion $k\rho >> 1$ is dominant for this case. The effect of decreasing the element length is illustrated in figures 4 through 6 in which the element length is decreased from 1500 m to 150 m to 15 m, respectively.

In the limit of very high frequency (high enough so that only the radiation terms in the exact solution need be considered), both solutions predict power spectra which are proportional to $| \tilde{f}(\nu) |$ times an oscillating factor. In the exact solution, this factor oscillates between finite upper and lower limits determined by the geometry; in the far-field solution, this oscillation is $\sin [\frac{1}{2}kL(1 - \hat{\ell} \cdot \nabla\rho_c)]$ and, in particular, has nulls that are not usually present in the exact solution. On the other hand, the peak values predicted by the two solutions are essentially the same whenever the length of the filament is short enough so that $\rho_a \cong \rho_b$. Therefore, if only the upper envelope of the magnitude of the power spectrum is required, it is proportional in both cases to $| \tilde{f}(\nu) |$, and the criterion that the proportionality constants be equal is that, for i = a,b:

$$\frac{1}{\rho_i}\sqrt{\frac{1+\hat{\ell}\cdot\nabla\rho_i}{1-\hat{\ell}\cdot\nabla\rho_i}}\;\hat{\epsilon}(\rho_i)\cdot\hat{z}\simeq\frac{1}{\rho_c}\sqrt{\frac{1+\hat{\ell}\cdot\nabla\rho_c}{1-\hat{\ell}\cdot\nabla\rho_c}}\;\hat{\epsilon}(\rho_c)\cdot\hat{z} \qquad (32)$$

which is independent of frequency. This requirement will be satisfied if $L/\rho_c \ll 1$. Therefore, although the requirement $kL^2/\rho \ll 1$ would indicate a failure of the far-field solution at large k, this does not happen if only the upper envelope of the power spectrum is required. In this case, the purely geometric criterion given in equation 32 is appropriate.

The high-frequency behavior of the exact and approximate solutions are illustrated in figures 9 and 10. Again the three-exponential waveform (Appendix A) has been used, and the observer is located on the surface at 10 km from the origin. In figure 9, the filament is vertical, 1.5 km long with one end at the origin. In figure 10, the filament is horizontal with its center 4 km above the surface at the origin and oriented so that the filament and observer are coplanar. Note that the exact and approximate solutions are essentially identical for frequencies above about 1 kHz ($k\rho = 1$). (Nulls in the approximate solution do not show in the plot because of computer sampling and roundoff errors.) The different slope of the spectra for the horizontal and vertical elements is attributable to the factor, $L(1 - \hat{\ell}\cdot\nabla\rho)$—the effective length of the filament which is essentially L for the vertical element, but is considerably smaller for the horizontal element. Note that, for the vertical element, no apparent difference exists between the exact and approximate solutions (except near the nulls), even at frequencies above 1 MHz where the requirement, $kL^2/\rho \ll 1$, is no longer valid.

EXAMPLES OF SPECTRA

The actual spectrum measured by the observer depends on the orientation of the current element, the polarization of the observer's receiver, and the height of the observer above the surface, as well as the physical properties of the filament (i.e., current waveform, velocity of propagation, and element length). This section contains examples that illustrate the effects of some of these factors on the observed spectrum.

The word "spectrum" is used here to mean "Fourier transform." Because all of the analysis presented in this document is in the frequency domain, the Fourier transform has already been taken as part of the solution. The figures presented here are plots of the magnitude of the spectrum (in dB) versus frequency (in Hz). That is, 20 times the logarithm (base 10) of the magnitude of a particular electric field component is plotted on the ordinate versus frequency on the abscissa. Therefore, if the spectrum of the x-component of electric field is being presented, $20 \log [E_x(\nu)\, E_x^*(\nu)]$ will be plotted against frequency in hertz (Hz).

At very high frequency, the spectra oscillate rapidly, causing a problem in the graphical presentation of the results. In particular, as the frequency increases, the resolution (i.e., size of the scale) required for resolving these oscillations must also increase. If a fixed scale size and a fixed sampling interval are held for the machine calculations, aliasing can occur because the results are eventually under-sampled. This happens in most of the figures shown

here in which data points at frequencies greater than about 1 MHz are shown, and is especially evident in figures 9, 11, and 14. In general, the high-frequency results presented here accurately represent the (upper) envelope of the spectrum, but not the location or number of nulls or maxima. Although the algorithms developed for this analysis are capable of including the location or number of nulls or maxima, the graphs would have been of impractical size. The actual spacing of nulls is discussed in Appendix A.

Observer's Orientation

When the observer is on the surface, only a z-component of electric field is measured. However, when the observer moves above the surface (for example, onto an elevated platform or aboard an airplane), other components of the electric field are observed. This effect is illustrated in figures 11 through 13, in which a vertical element 1.5 km long with one end at the origin is treated for an observer 100 km from the origin but at angles of 65, 40, and 15 degrees with respect to the vertical (i.e., axis of the filament). The filament and the observer were chosen to be coplanar in all of these cases so that only two components of electric field would need to be plotted. The curve labeled E(x) corresponds to a radially (i.e., perpendicular to the z-axis) directed field component. For comparison, figure 9 shows the observer located on the surface (90 degrees from the vertical). Note that, as the observer approaches the axis of the filament, the spectrum becomes flatter (the peak near 10 kHz begins to disappear) and there is a general shift toward higher frequency and larger amplitude. This effect is caused by changes in the effective filament length $L(1 - \hat{\ell} \cdot \nabla\rho)$ which can differ significantly from the filament's physical length, L, whenever $\hat{\ell} \cdot \nabla\rho = 1$.

Figures 14 through 16 show the spectrum of the electric field components radiated by a horizontal current element 1.5 km long with its center 4 km above the origin and parallel to the x-axis. The observer is again about 100 km away from the filament and lies in a plane that contains the filament and the z-axis; however, the observer is oriented so that the position vector of the observer (the line from the origin to the observer) makes angles of 15, 40, and 65 degrees (figures 14 through 16, respectively) with respect to the vertical.

Because of symmetry, only two components of electric field exist for this particular orientation—the x- and z-components. However, if the observer moves out of the x-y plane so that the observer's position vector and the filament are no longer coplanar, all three rectangular field components may exist. Figures 17 and 18 show examples of such cases for a 1.5-km long horizontal current filament centered 4 km above the origin and parallel to the x-axis. The observer is about 100 km away. In figure 17, the observer is on the y-z plane at (y = 90.63 km; z = 42.26 km) so that the position vector of the observer makes an angle of about 75 degrees with the vertical. In figure 18, the observer is located at (x = 50 km; y = 30 km; z = 2 km).

Effect of Distance

The effect of the distance of the observer from the filament is to generally decrease the amplitude of the spectrum measured by the observer. This is illustrated in figures 19 through 21

using the exact solution, and in figures 22 through 24 using the approximate solution. The calculations were made for a 1.5-km long vertical element, with one end at the origin and the observer along a line in the z-x plane which makes an angle of about 1.15 degrees with the x-axis. Note the decrease in amplitude with an increase in distance and the general improvement in the agreement of the exact and approximate solutions as the distance of the observer from the filament increases. As this distance increases, the criterion, $k\rho \gg 1$, can be satisfied at lower frequencies, extending the range of agreement between the exact and approximate solutions to lower frequencies.

Orientation of the Current Element

In most of the preceeding examples, the current element has been vertical with one end located on the surface. Although this geometry is apropos of nearly vertical return strokes, it is not necessarily representative of other elements of the lightning flash, such as the individual steps in the stepped leader or of intercloud strokes. Figures 25 through 27 show spectra which are the result of a filament 1.5 km long with its center 4 km above the surface. The observer was located on the surface, 100 km from the origin. The element and observer are coplanar, but the angle that the element makes with the vertical is 45 degrees in figure 25 and -45 degrees in figure 27; in figure 26 the element is vertical. The case of a horizontal element has already been given for this geometry in figure 9. Again note the broadening of the spectrum and the shift toward higher frequencies because of changes in the effective length, $L(1 - \hat{\ell} \cdot \nabla\rho)$, or in the orientation of the filament.

Effect of Velocity of Propagation

The velocity with which the current wave propagates along the filament has a definite effect on the fields radiated by the element. This effect is demonstrated in figures 28 through 30 in terms of the approximate (i.e., far-field) solution which, unlike the exact solution, applies to all velocities of propagation. In each case shown in the figures, the filament is vertical with one end at the origin and is 1.5 km long, and the observer is located on the surface 10 km from the origin. Figure 28 shows the electric field measured by the observer for the case in which the velocity of propagation, v, equals the speed of light in vacuum, c. In figure 29, $v = c/10$, and in figure 30, $v = c/100$.

As can be seen, the effect of decreasing the velocity of propagation is to shift the peak in the spectrum toward lower frequency with only minor changes in the overall shape. However, if ν becomes so small that the peak is shifted well beyond the knee of $f(\nu)$ (figure 8), a change in the shape of the spectrum can also be expected.

The magnitude of the spectrum of the electric field as predicted by the approximate solution for an observer on the surface is (equation 28a):

$$\sqrt{\tilde{\bar{E}}(\bar{r}_o, \nu) \cdot \tilde{\bar{E}}^*(\bar{r}_o, \nu)} = \frac{\sqrt{\mu/\epsilon}}{\rho_c} |\tilde{f}(\nu)| \frac{1 - (\hat{\ell} \cdot \nabla\rho_c)^2}{\eta - (\hat{\ell} \cdot \nabla\rho_c)} \sin\left[\frac{kL}{2}(\eta - \hat{\ell} \cdot \nabla\rho_c)\right]$$

In the case of $\hat{\ell} \cdot \nabla p_c << 1$, which is reasonable for a distant observer and a vertical element, the frequency dependence is roughly: $| \tilde{f}(\nu) | \sin(\eta\, kL)$. That is, the spectrum depends on a factor that scales in frequency as $k\eta$ for fixed L and is multiplied by a factor dependent on the waveform (figures 28 through 30).

TRANSFER FUNCTION FOR THE RADIATION PROCESS

Examination of the solutions for the radiated fields (i.e., equations 11 and 15 for the exact solution or equations 31 for the approximate solution) indicates that they may be written in the form:

$$\tilde{\bar{E}}(\bar{r}_o, \nu) = \tilde{f}(\nu)\, \tilde{\bar{h}}_e(\bar{r}_o, \nu) \tag{33a}$$

$$\tilde{\bar{H}}(\bar{r}_o, \nu) = \tilde{f}(\nu)\, \tilde{\bar{h}}_h(\bar{r}_o, \nu) \tag{33b}$$

where $f(\nu)$ is the Fourier transform of the shape of the disturbance that propagates down the filament, and $\tilde{\bar{h}}_{e,h}(r_o, \nu)$ is a vector function that depends on the observer-filament geometry and on the physical properties of the filament (such as length, orientation, and velocity of propagation) but not on the current waveform. Consequently, the radiation problem is considered to be a linear system in which $f(\nu)$ is the input current waveform, $\tilde{\bar{h}}_{e,h}(\bar{r}_o, \nu)$ is the transfer function for the "system," and $\tilde{\bar{E}}(\bar{r}_o, \nu)$ or $\tilde{\bar{H}}(\bar{r}_o, \nu)$ is the output. The requirement, inherent in the derivations, that the waveform propagate along the channel, is a characteristic that belongs to the system (i.e., all $f(\nu)$ propagate).

Examples of the modulus of the vector components of the transfer function are shown in figures 31 through 35 for a vertical element 1.5 km long with one end at the origin. In figure 32, the observer is on the surface, 100 km form the origin. In this case, only the z-component of the transfer function is nonzero, and this component is plotted in the figure for both the approximate and the exact solutions. In figures 32 through 34, the observer is also 100 km from the filament, but it is located so that the position vector of the observer makes angles of 65, 40, and 15 degrees, respectively, with respect to the vertical.

Note that, for high enough frequency, the transfer function becomes oscillatory with a constant maximum value for both the approximate and the exact solutions; however, the lower bound (not shown in the figures) is zero for the approximate solution and is finite for the exact solution (Appendix D). It follows that, at sufficiently high frequency, the envelope of the spectrum is determined by the current waveform, independent of geometry. At lower frequencies, both geometry and the current waveform affect the shape of the spectrum.

Goddard Space Flight Center
National Aeronautics and Space Administration
Greenbelt, Maryland September, 1976

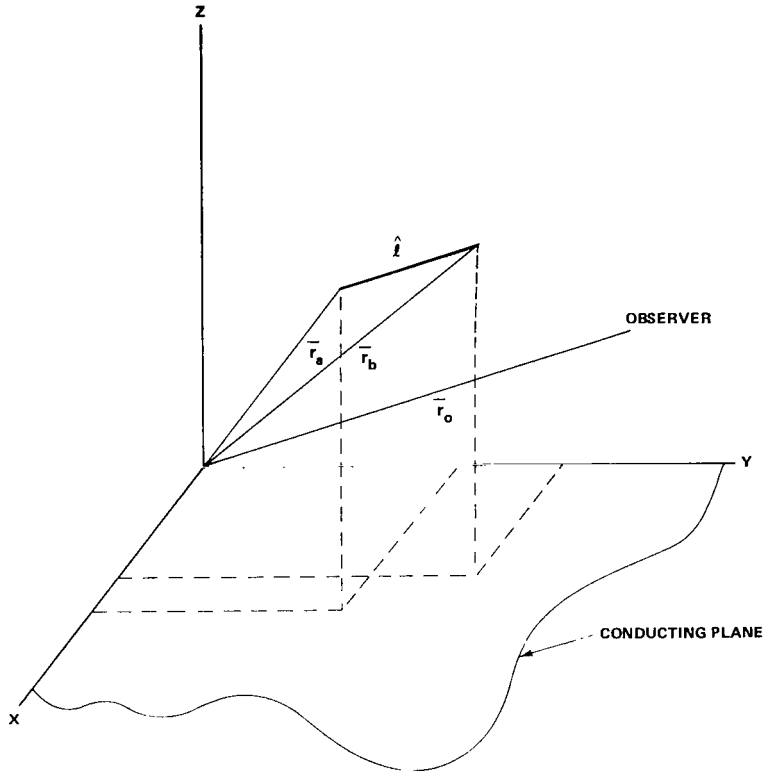

Figure 1. Geometry for the calculation.

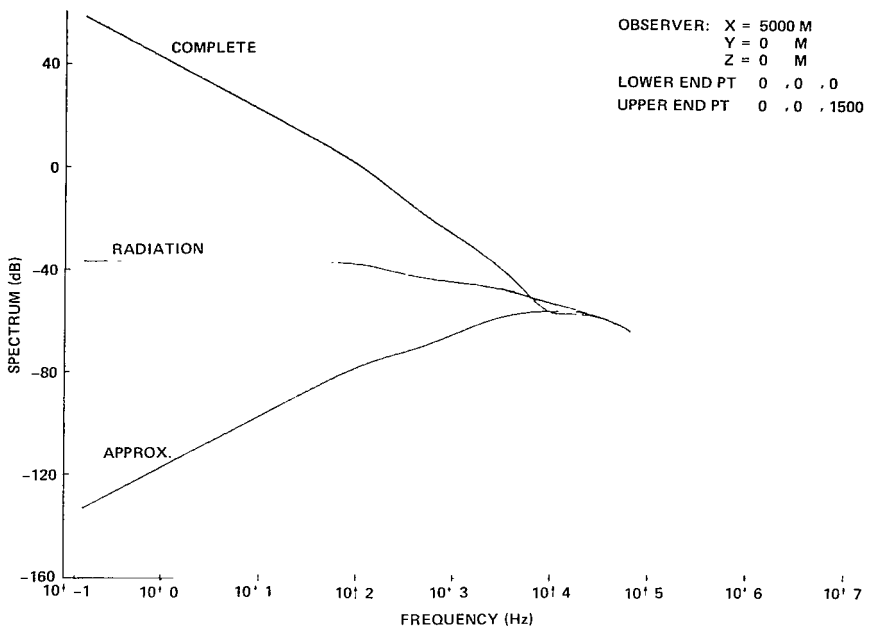

Figure 2. Low-frequency behavior of exact and approximate solutions.

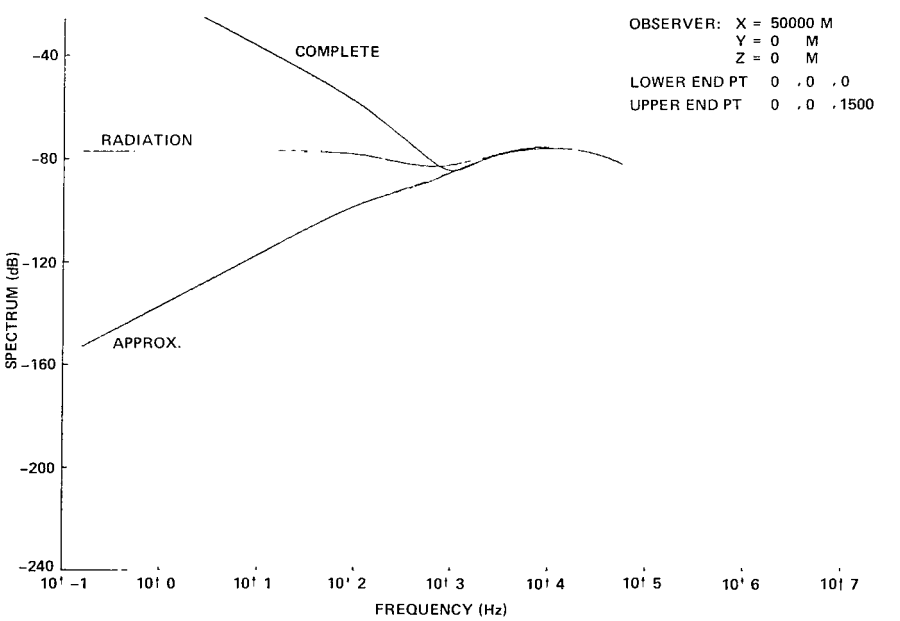

Figure 3. Low-frequency behavior of exact and approximate solutions.

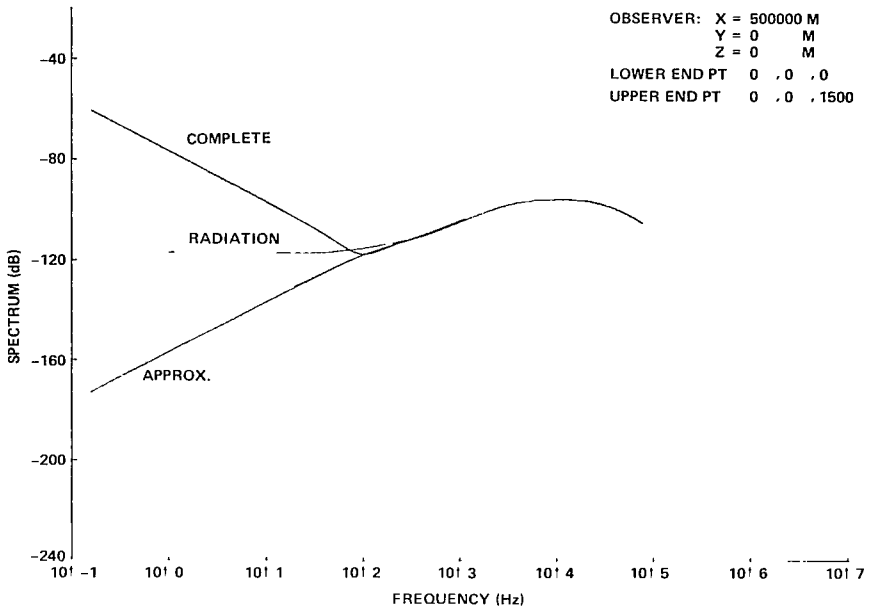

Figure 4. Low-frequency behavior of exact and approximate solutions.

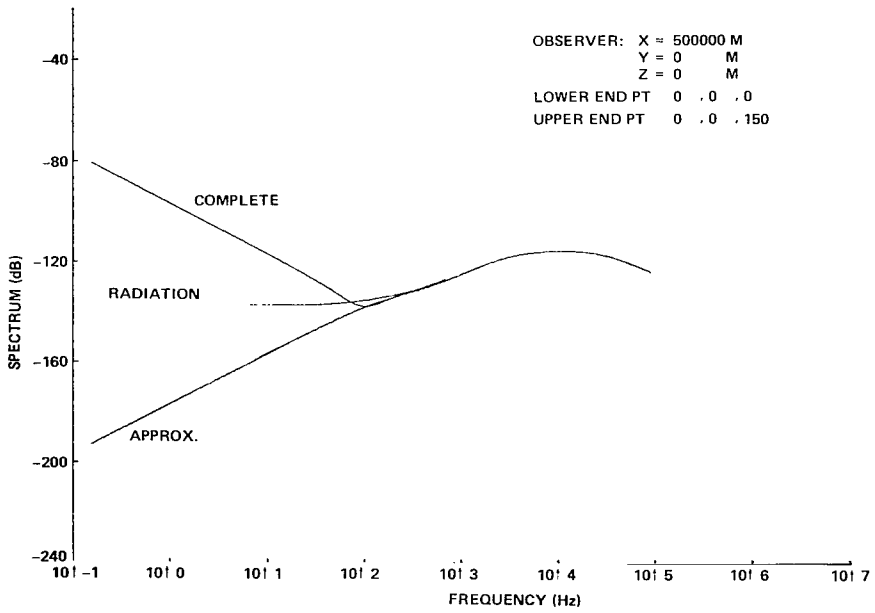

Figure 5. Low-frequency behavior of exact and approximate solutions.

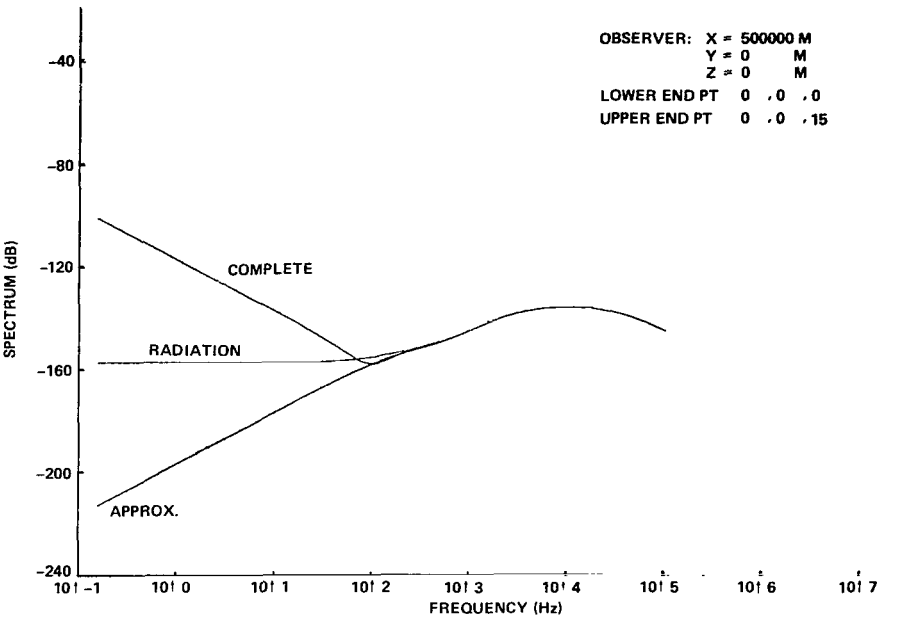

Figure 6. Low-frequency behavior of exact and approximate solutions.

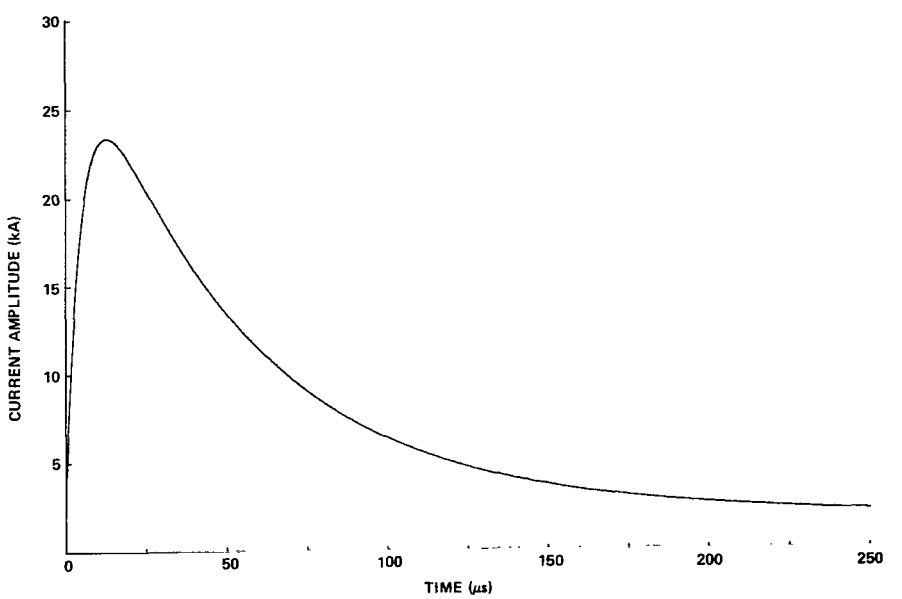

Figure 7. Current waveform.

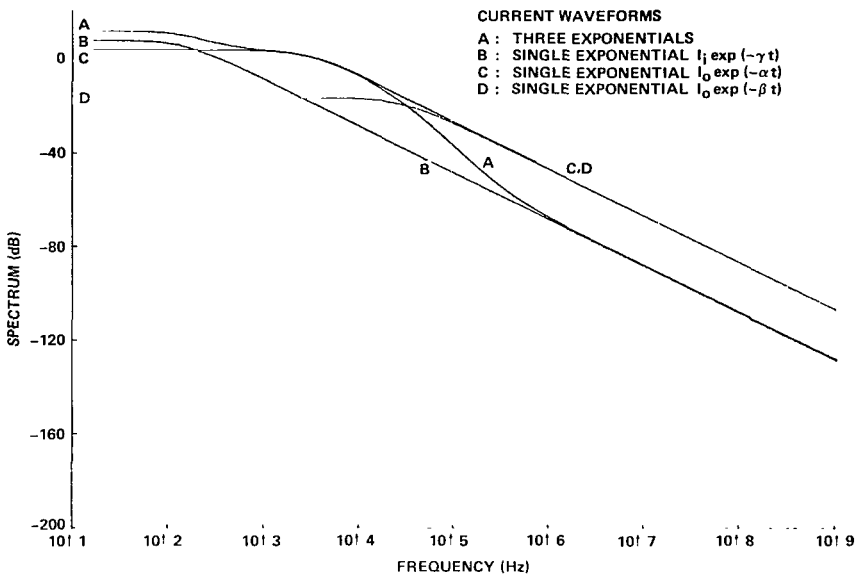

Figure 8. Spectrum of current waveform.

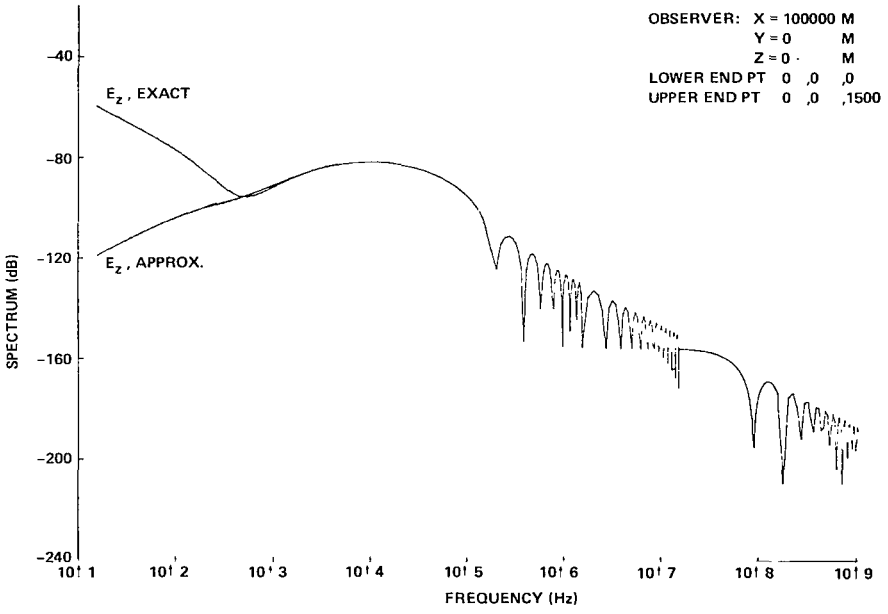

Figure 9. Exact and approximate solutions: three-exponential waveform.

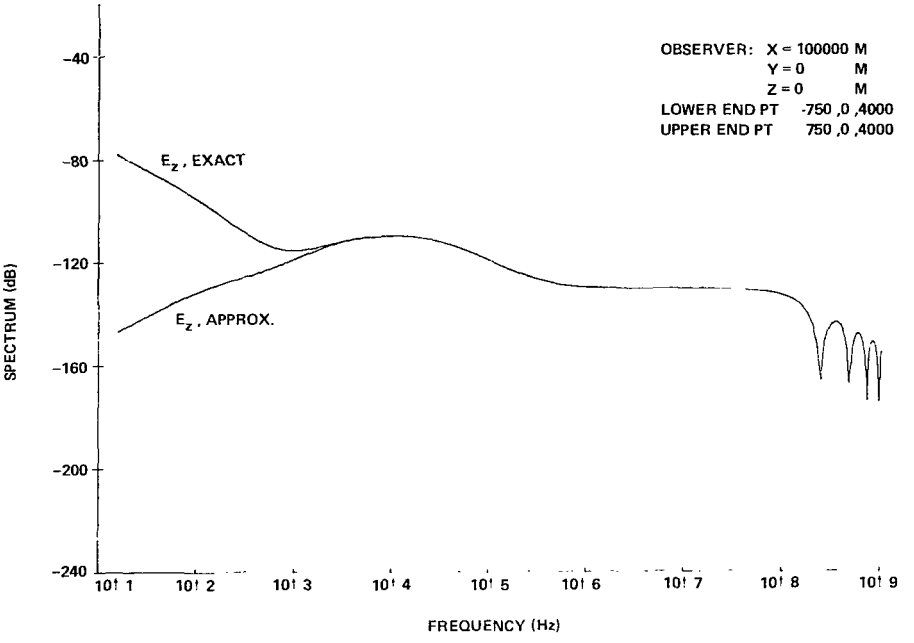

Figure 10. Exact and approximate solutions: three-exponential waveform.

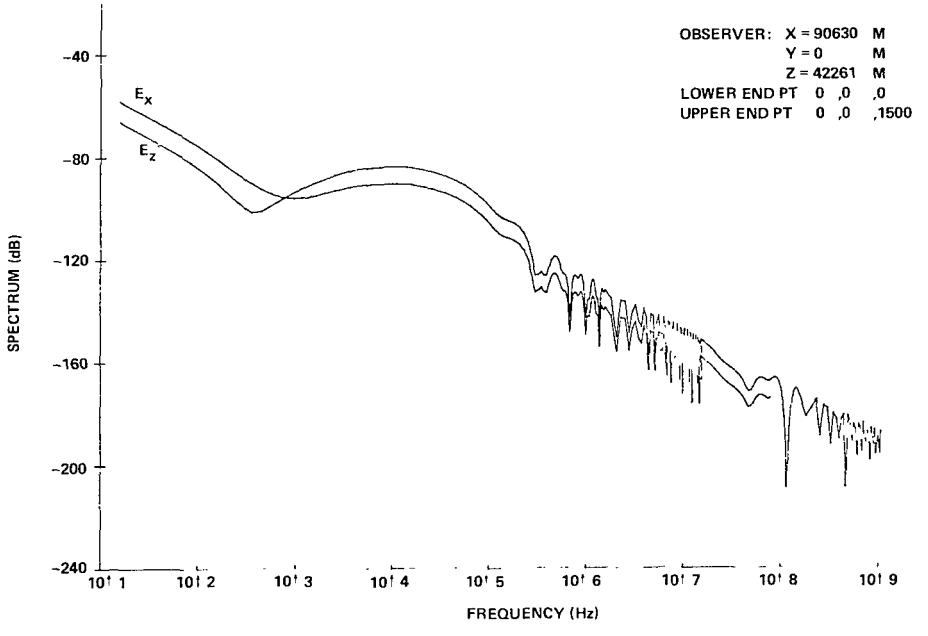

Figure 11. Exact solution: three-exponential waveform.

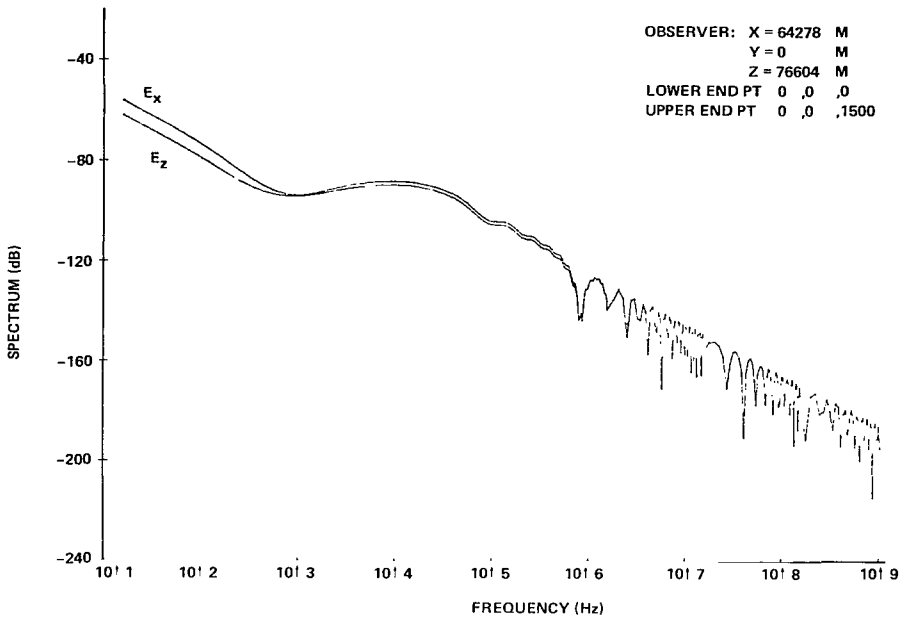

Figure 12. Exact solution: three-exponential waveform.

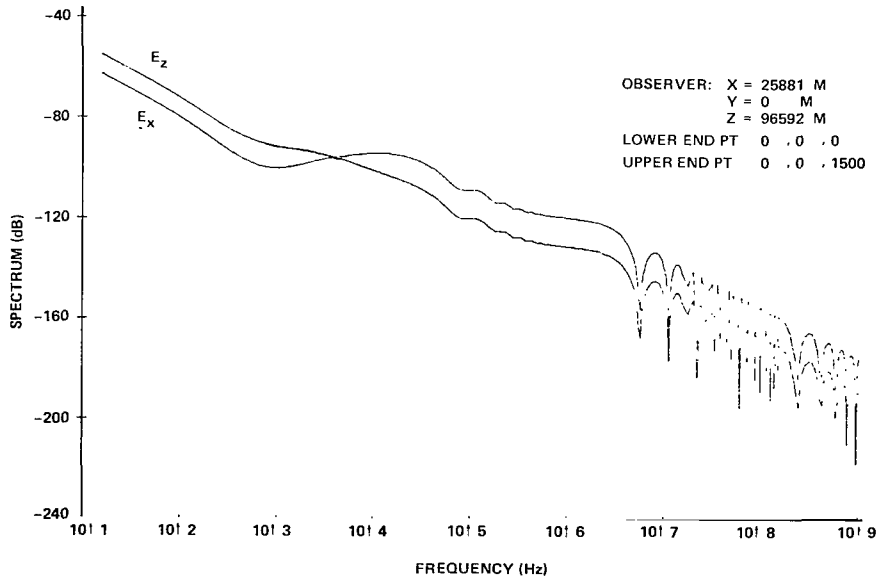

Figure 13. Exact solution: three-exponential waveform.

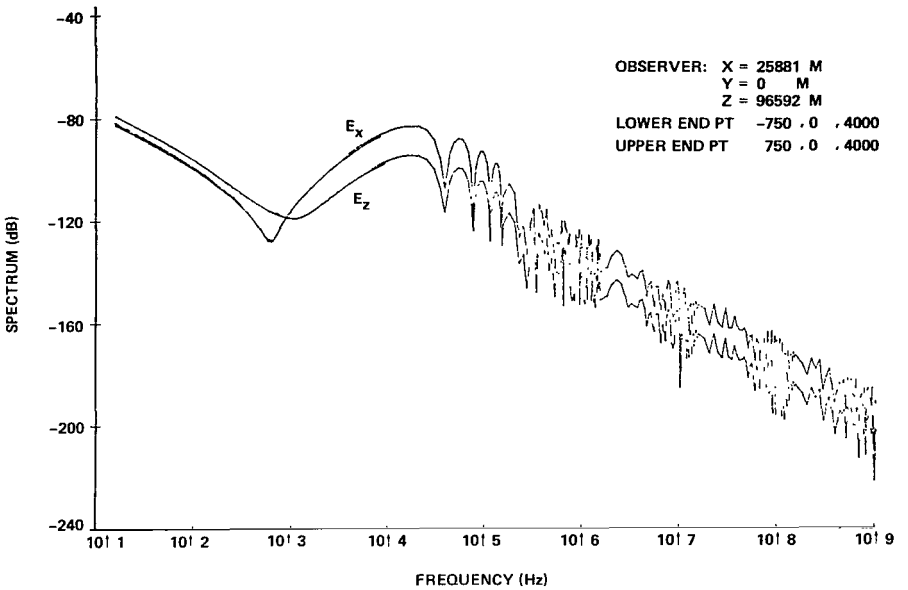

Figure 14. Exact solution: three-exponential waveform.

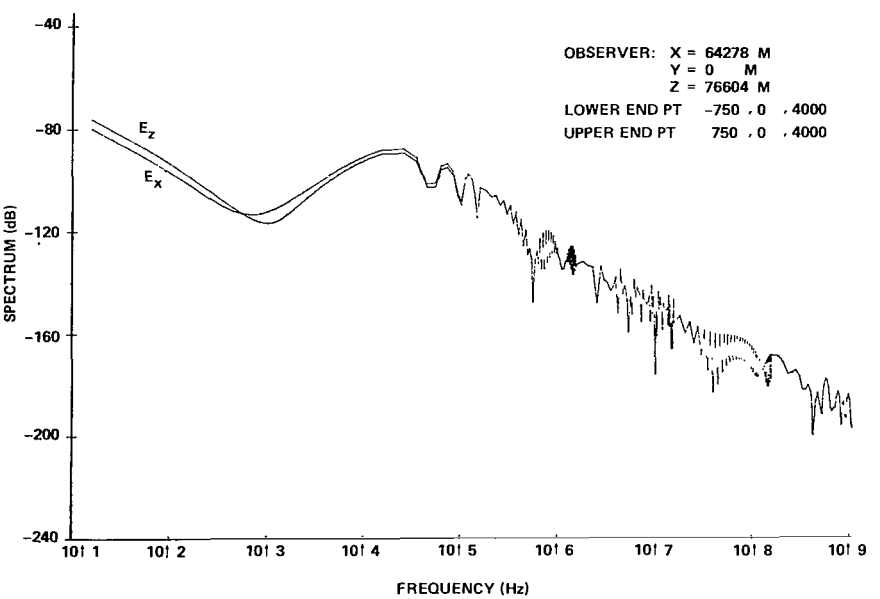

Figure 15. Exact solution: three-exponential waveform.

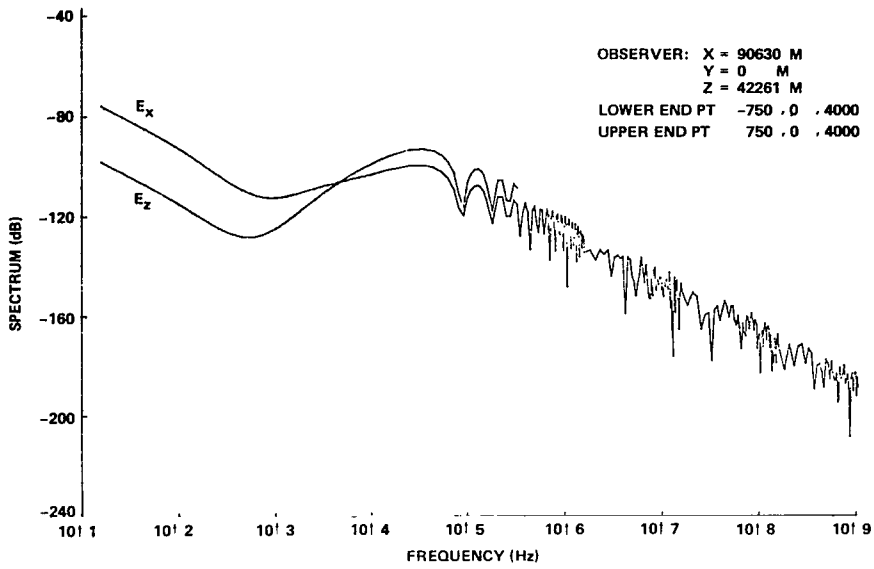

Figure 16. Exact solution: three-exponential waveform.

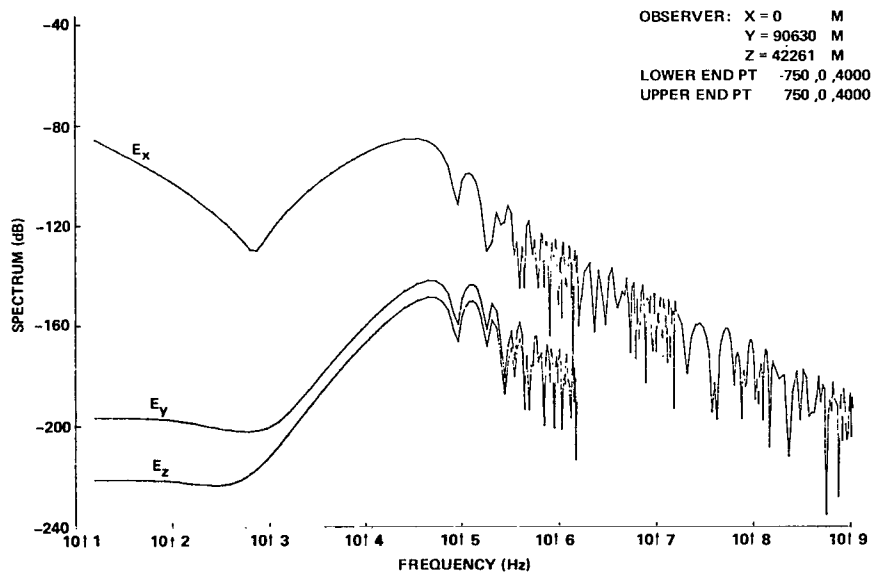

Figure 17. Exact solution: three-exponential waveform.

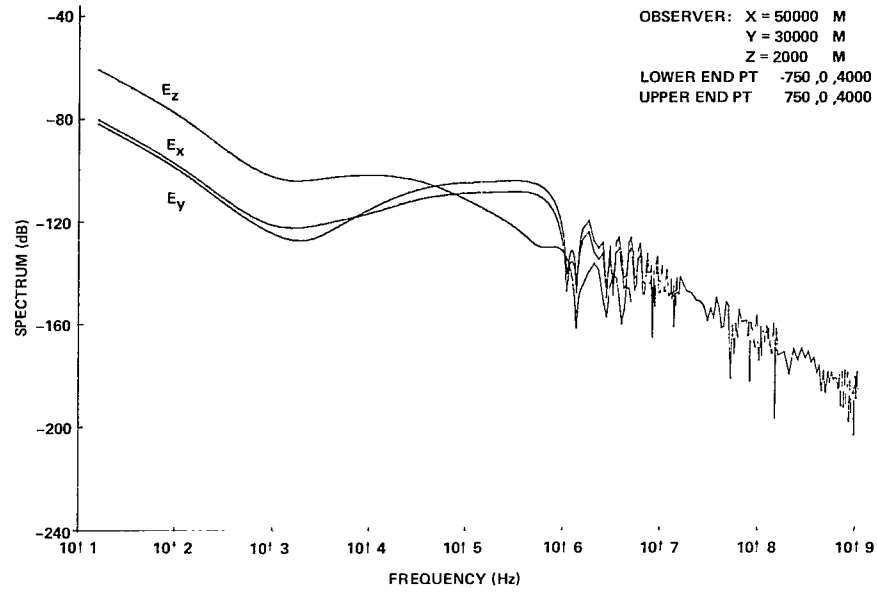

Figure 18. Exact solution: three-exponential waveform.

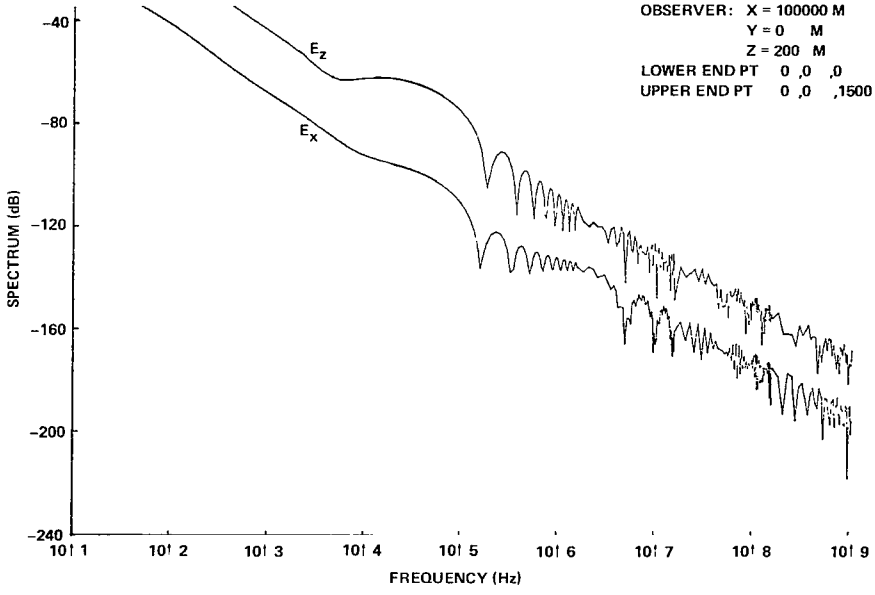

Figure 19. Exact solution: three-exponential waveform.

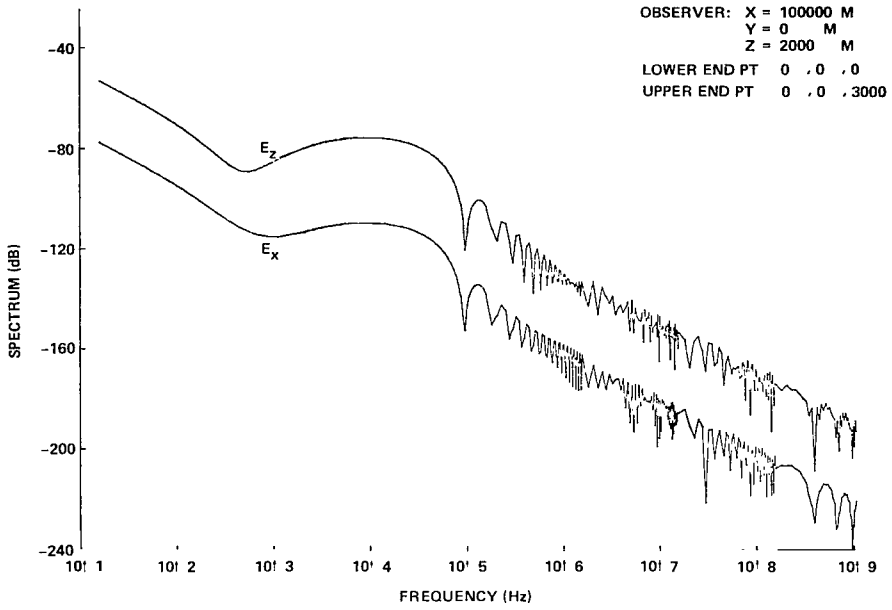

Figure 20. Exact solution: three-exponential waveform.

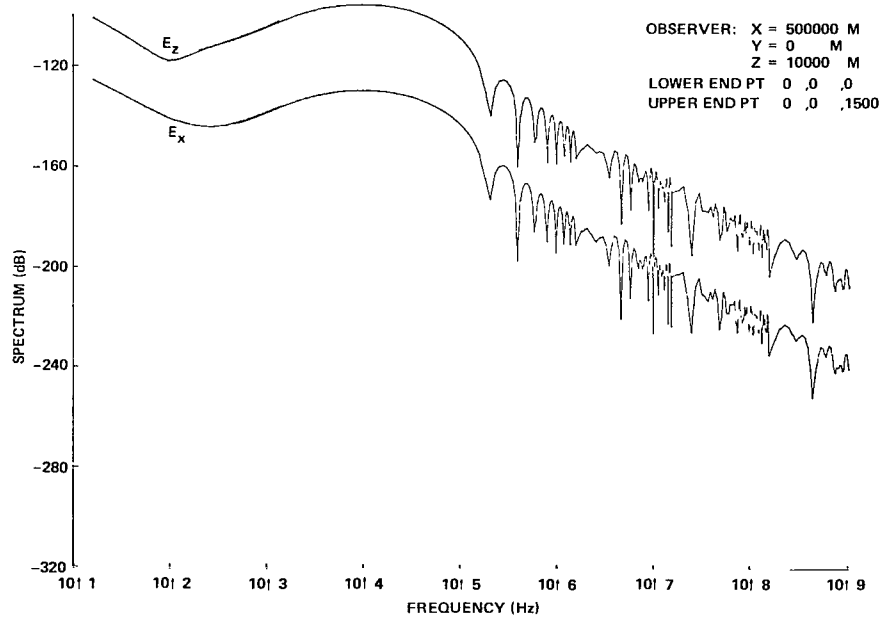

Figure 21. Exact solution: three-exponential waveform.

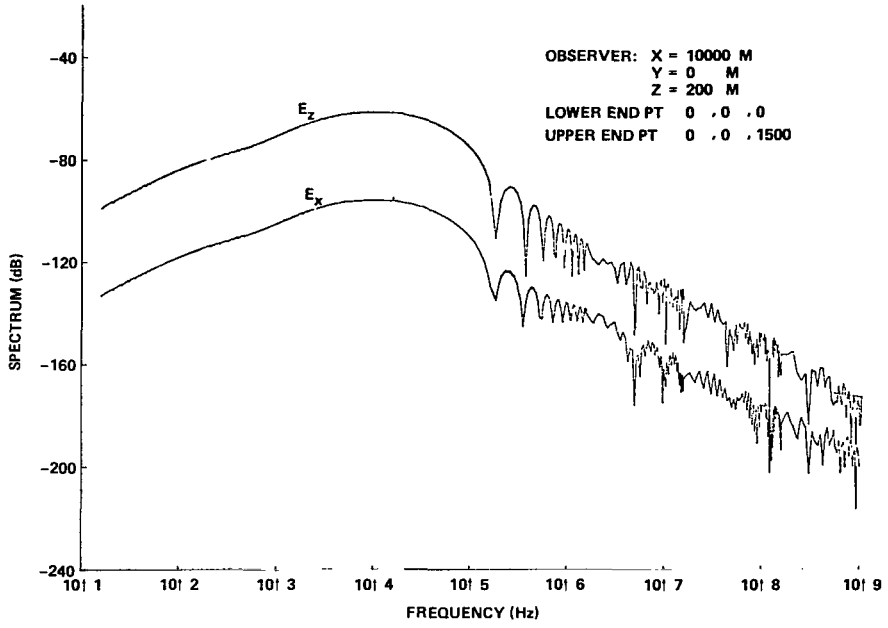

Figure 22. Approximate solution: three-exponential waveform.

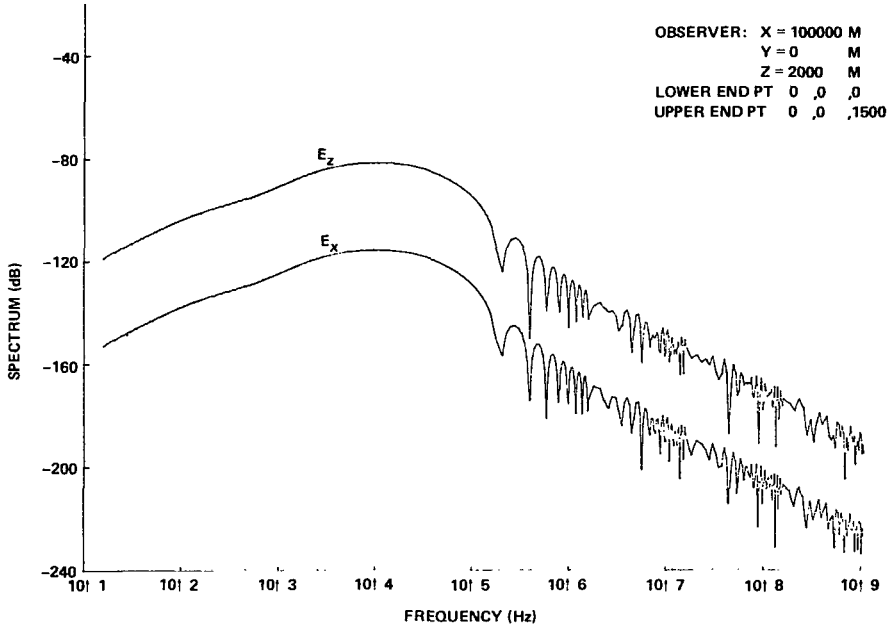

Figure 23. Approximate solution: three-exponential waveform.

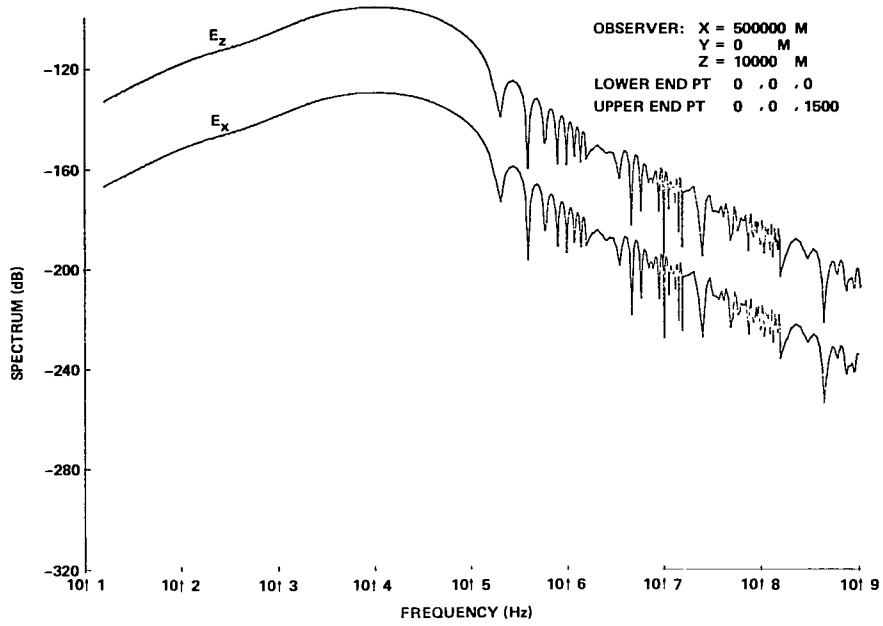

Figure 24. Approximate solution: three-exponential waveform.

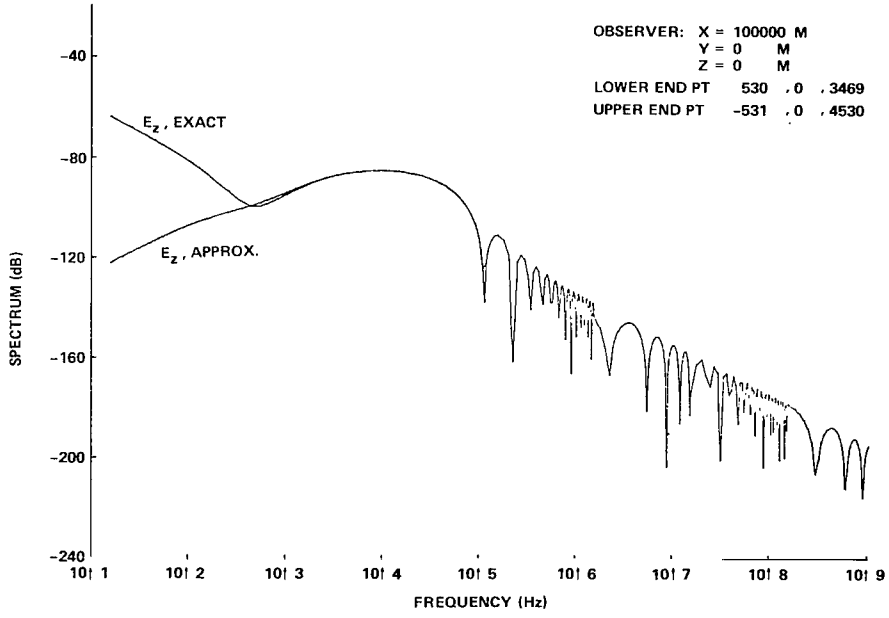

Figure 25. Exact and approximate solutions: three-exponential waveform.

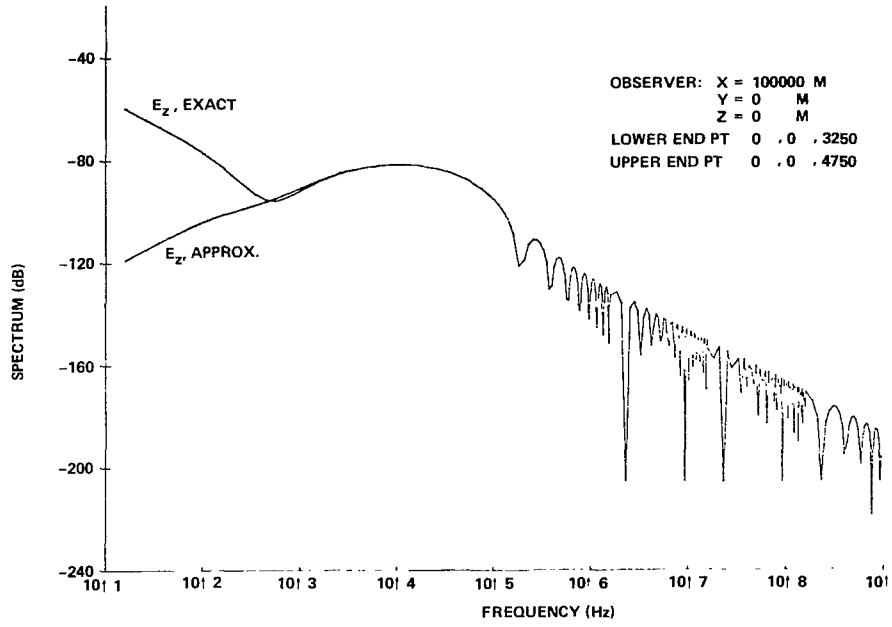

Figure 26. Exact and approximate solutions: three-exponential waveform.

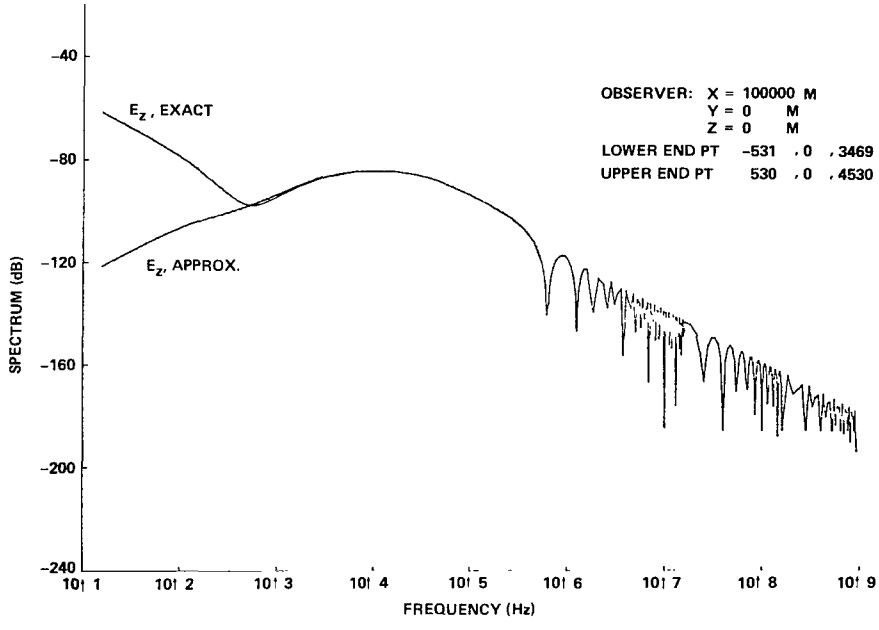

Figure 27. Exact and approximate solutions: three-exponential waveform.

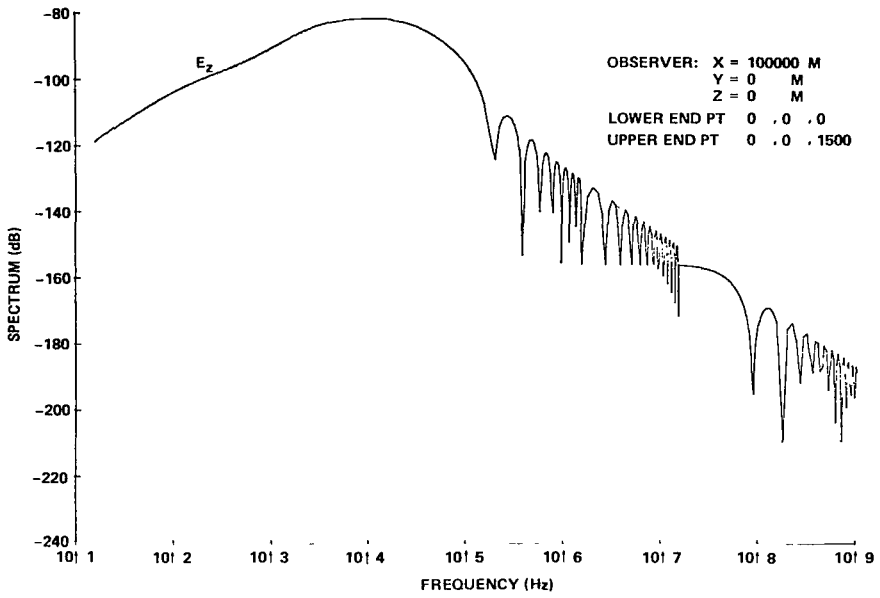

Figure 28. Approximate solutions: three-exponential waveform, V = C.

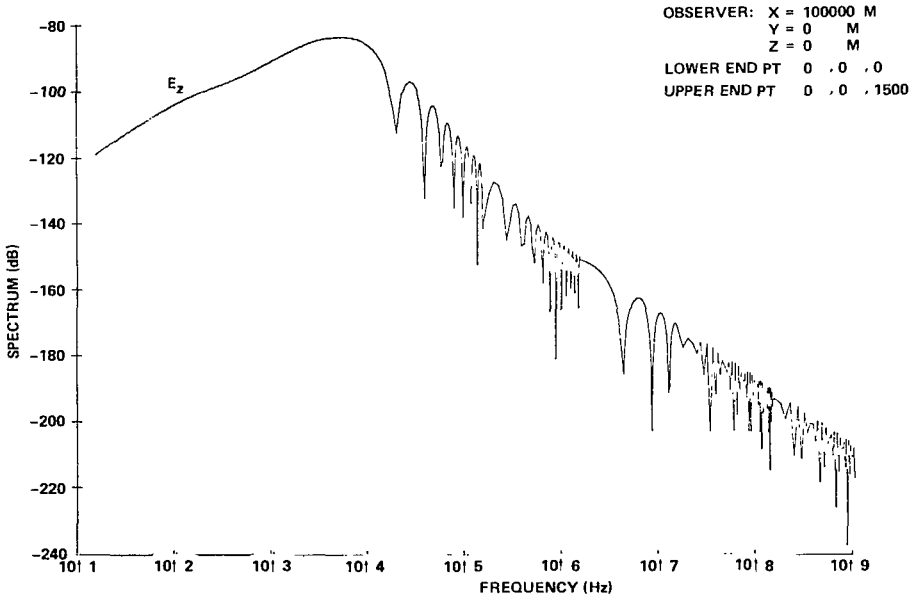

Figure 29. Approximate solution: three-exponential waveform, V = C/10.

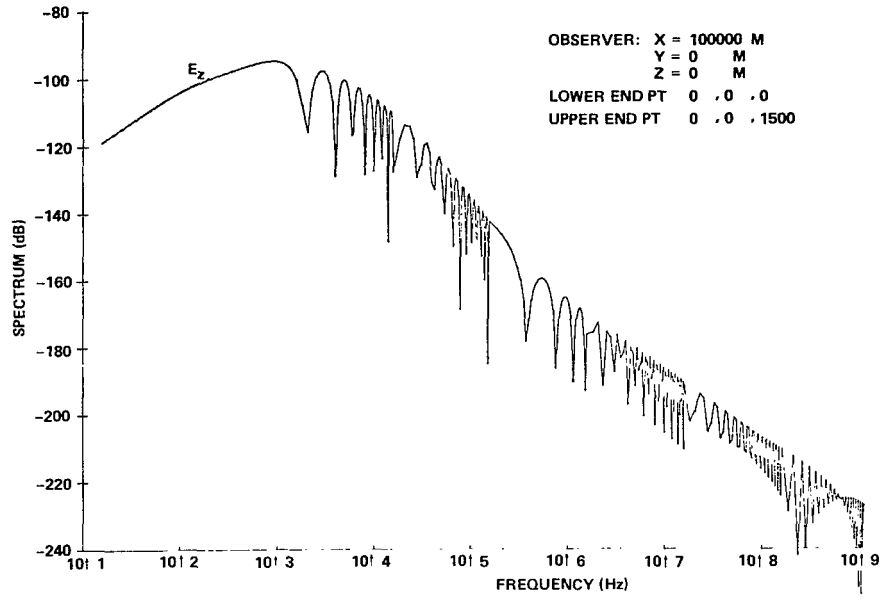

Figure 30. Approximate solution: three-exponential waveform, V = C/100.

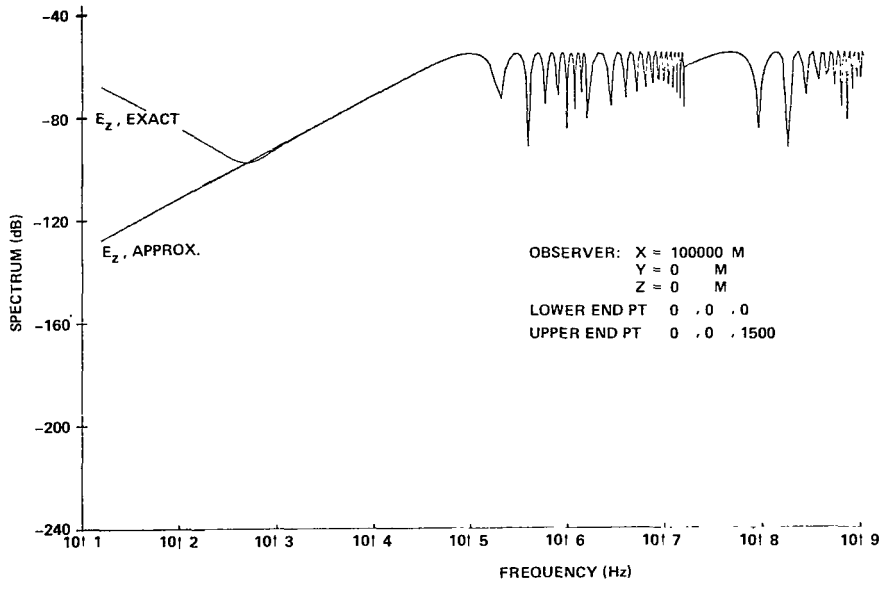

Figure 31. Exact and approximate solutions: three-exponential waveform, f (ν) = constant.

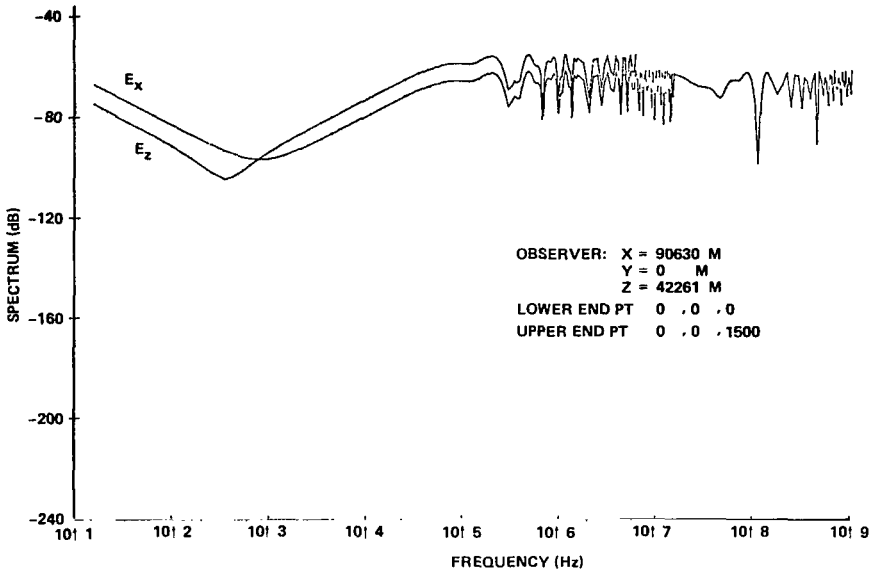

Figure 32. Exact solution: three-exponential waveform, f (ν) = constant.

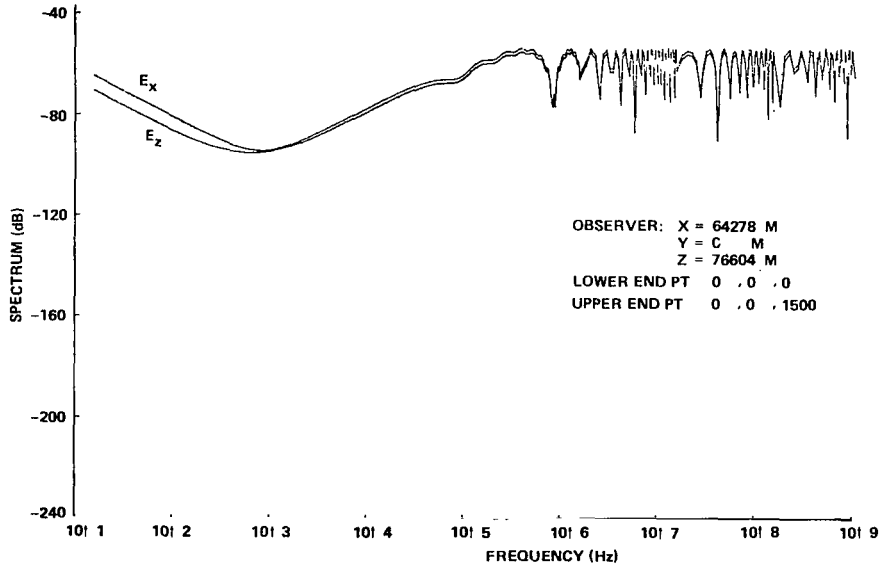

Figure 33. Exact solution: three-exponential waveform, f (ν) = constant.

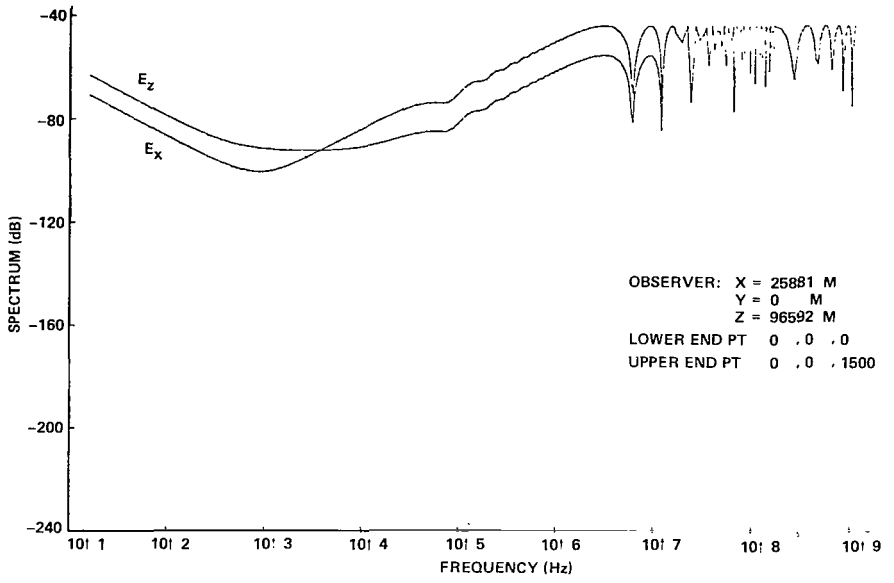

Figure 34. Exact solution: three-exponential waveform, f (ν) = constant.

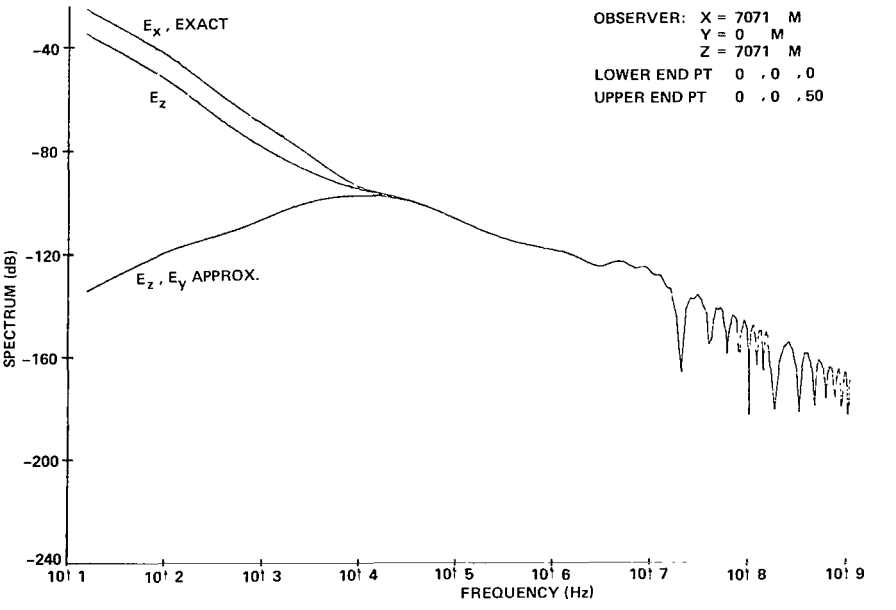

Figure 35. Exact and approximate solutions: three-exponential waveform.

REFERENCES

1. Taylor, W. L., "Atmospherics and Severe Storms," Chapter 17 in *Remote Sensing of the Troposphere*, V. E. Derr, ed., USGPO, 1972.

2. Jones, H. L., "A Sferics Method of Tornado Identification and Tracking," Bull. Am. Meteorol. Soc. (32) 1951, pp. 380-385.

3. Jones, H. L., and P. Hess "Identification of Tornadoes by Observation of Waveform Atmospherics," Proceedings of the IRE, **40**, 1952, pp. 1049-1052.

4. Uman, M., *Lightning*, Chapter 4. McGraw-Hill, New York, 1969.

APPENDIX A
CURRENT WAVEFORM

APPENDIX A

CURRENT WAVEFORM

Measurement of the current in return strokes reveals that the current pulse has a sharp rise time (on the order of microseconds to peak value) followed by a relatively slow decay (on the order of 50 to 100 microseconds), and a small residual current (continuing current) that can persist for hundreds of microseconds after the main pulse is over. A combination of three exponentials is common in the literature on lightning for modeling this current (References 1, 2, and 3). Consequently, such a model has been adopted for use here.

The following model is taken from Reference 1:

$$I(t) = I_0 \left[e^{-\alpha t} - e^{-\beta t} \right] + I_1 e^{-\gamma t} \tag{A1}$$

where, for a typical lightning return stroke, the parameters are:

$$\alpha = 2.0 \times 10^4 \tag{A2}$$

$$\beta = 2.0 \times 10^5 \tag{A3}$$

$$\gamma = 1.0 \times 10^3 \tag{A4}$$

$$I_0 = 30 \text{ ka} \tag{A5}$$

$$I_1 = 2.5 \text{ ka} \tag{A6}$$

The first two exponentials in equation A1 represent the main current pulse, and the third term, $I_1 \exp(-\gamma t)$, represents the continuing current. The current waveform, as predicted by this model, is as shown previously in figure 7. Note that the peak occurs about 13 microseconds after initiation of the pulse.

The spectrum of I(t), which is denoted $\tilde{f}(\nu)$ in the text, was shown previously in figure 8. Twenty times the logarithm (to base 10) of the magnitude of the Fourier transform of I(t) is plotted (along the ordinate) versus frequency (along the abscissa). Curve A represents $|\tilde{f}(\nu)|$, and curves B, C, and D represent the (magnitude of) Fourier transform of the three constituent exponentials: $I_o \exp(-\alpha t)$, $I_o \exp(-\beta t)$, and $I_1 \exp(-\gamma t)$, respectively.

This current waveform has been used in all of the computations made in the text. It is reasonably representative of the actual current in return strokes, and consequently, the results presented here should be reasonable in a quantitative sense for the fields radiated by the return stroke. The currents carried by other components of the lightning flash (stepped leader, dart leader, and intercloud processes) are not as well known and probably differ

from I(t), at least in magnitude (i.e., I_o) if not in shape. Consequently, the results predicted here would probably be less quantitatively correct when applied to flash elements other than return strokes. On the other hand, the analysis is independent of I(t), and, after sufficient information is obtained to model I(t) for a given process, the formalism presented here can be adopted without change to produce the radiated fields.

Note that, in the computations of spectra made in the text, it is assumed that the current waveform propagates along the channel (filament). That is, the current is $I(t - \hat{\ell} \cdot r/v)$, which is a wave that travels in the $\hat{\ell}$ direction with speed, v.

REFERENCES

1. Uman, M., *Lightning*, Chapter 4, McGraw-Hill, New York, 1969.
2. Dennis, A. S., and E. T. Pierce, "The Return Stroke of the Lightning Flash to Earth as a Source of VLF Atmospherics," *Radio Science*, 68D (7), 1964, pp. 777-794.
3. Bruce, C. E. R., and R. N. Gold, "The Lightning Discharge," JIEE (London) 80 (II), 1941, pp. 487-505.

APPENDIX B
COORDINATE TRANSFORMATION

APPENDIX B

COORDINATE TRANSFORMATION

The objective of this appendix is to present a rotation of coordinates that will permit the z-axis of the reference coordinate system (x, y, z) to be aligned with an arbitrary unit vector, $\hat{\ell}$. One way to accomplish this transformation is to first rotate in the counterclockwise direction about the original z-axis through an angle, $\theta = \tan^{-1}\ [\ \ell_x/\ell_y\ ]$, until the x-axis of the original system and the projection of $\hat{\ell}$ on the x-y plane are colinear. The matrix for this rotation is:

$$\left[R_\theta\right] = \begin{bmatrix} 0 & \sin\theta & \cos\theta \\ 0 & \cos\theta & -\sin\theta \\ 1 & 0 & 0 \end{bmatrix} \qquad \text{(B1)}$$

Next, a counterclockwise rotation is made through the angle,

$$\phi = \tan^{-1}\left[\frac{\sqrt{\ell_x^2 + \ell_y^2}}{\ell_z}\right]$$

about the new y-axis until the z-axis is aligned with (colinear) the unit vector, $\hat{\ell}$. The matrix for this rotation is:

$$\left[R_\phi\right] = \begin{bmatrix} -\sin\phi & 0 & \cos\phi \\ 0 & 1 & 0 \\ \cos\phi & 0 & \sin\phi \end{bmatrix} \qquad \text{(B2)}$$

The total rotation matrix is $[R] = [R_{\phi}] [R_{\theta}]$. Thus, denoting the new coordinates by (x'', y'', z''),

$$\begin{bmatrix} x'' \\ y'' \\ z'' \end{bmatrix} = \begin{bmatrix} -\sin\phi & \cos\phi \sin\theta & \cos\phi \cos\theta \\ 0 & \cos\theta & -\sin\theta \\ \cos\phi & \sin\phi \sin\theta & \sin\phi \cos\theta \end{bmatrix} \begin{bmatrix} x \\ y \\ z \end{bmatrix} \qquad \text{(B3)}$$

The inverse matrix is the transpose of [R].

Of special interest is the transformation of the z-coordinate, which takes the form, $z'' = \hat{\ell} \cdot \overline{r}$, where $\overline{r} = (x\hat{x} + y\hat{y} + z\hat{z})$.

APPENDIX C
COMPLETE SOLUTION IN THE FRAUNHOFER REGION

APPENDIX C

COMPLETE SOLUTION IN THE FRAUNHOFER REGION

When $\rho_i >> L$, ρ_i may be expanded in a power series about the distance from the observer to the center of the current filament. Keeping only the first few terms,

$$\rho_i = |(\bar{r}_o - \bar{r}_c) + (\bar{r}_c - \bar{r}_i)|$$

$$\cong |\bar{r}_o - \bar{r}_c| + |\bar{r}_c - \bar{r}_i| \cos\phi_c + \frac{1}{2} \frac{|\bar{r}_c - \bar{r}_i|^2}{|\bar{r}_o - \bar{r}_c|} \tag{C1}$$

where

$$\cos\phi_c = \frac{(\bar{r}_c - \bar{r}_i) \cdot (\bar{r}_o - \bar{r}_c)}{|\bar{r}_c - \bar{r}_i| \quad |\bar{r}_o - \bar{r}_c|} \tag{C2}$$

and by noting that

$$\bar{r}_c - \bar{r}_i = \pm \frac{L}{2} \hat{\ell} \begin{cases} + \text{ for } i = a \\ - \text{ for } i = b \end{cases} \tag{C3}$$

the following form is obtained:

$$\cos\phi_c = \pm \hat{\ell} \cdot \nabla\rho_c \tag{C4}$$

where $\rho_c = |\bar{r}_o - \bar{r}_c|$ is the distance from the observer to the center of the filament.

Now, assume that ρ_c is sufficiently greater that L so that $\rho_i \simeq \rho_c$ in all terms in the expression for electric field except perhaps where it is multiplied by k, as in the exponentials,

exp(jk ρ_c); and assume that kL^2 / ρ_c is sufficiently small that the last (and all subsequent) terms in the expansion in equation C1 are negligible even in the exponentials. Then,

$$\frac{e^{jk\rho_i}}{4\pi\rho_i} \simeq \frac{e^{jk\rho_c}}{4\pi\rho_c} \exp\left[\pm jk\frac{L}{2}\hat{\ell}\cdot\nabla\rho_c\right] \tag{C5}$$

where the (+) pertains for i = a and the (-) for i = b. Finally, assume that k ρ_c is sufficiently large that only terms of lowest order in $1/k\rho_c$ need to be considered. Then, only the radiation terms in $\bar{\epsilon}(\rho_i)$ are significant and:

$$\frac{e^{jk\rho_i}}{4\pi\rho_i}\,\bar{\epsilon}(\rho_i) \simeq \frac{e^{jk\rho_c}}{4\pi\rho_c}\,\bar{\epsilon}_R(\rho_c)\exp\left[\pm j\frac{kL}{2}(1-\hat{\ell}\cdot\nabla\rho_c)\right] \tag{C6}$$

where the (+) is associated with i = b, and the (-) is associated with i = a, and

$$\bar{\epsilon}_R(\rho_c) = e^{jk\hat{\ell}\cdot\bar{r}_c}\sqrt{\frac{1+\hat{\ell}\cdot\nabla\rho_c}{1-\hat{\ell}\cdot\nabla\rho_c}}\,\hat{\epsilon}(\rho_c) \tag{C7}$$

The following relationship for $\hat{\ell}\cdot r_i$ has been employed:

$$\hat{\ell}\cdot\bar{r}_i = \hat{\ell}\cdot(\bar{r}_i - \bar{r}_c + \bar{r}_c)$$

$$= \hat{\ell}\cdot\bar{r}_c \pm \frac{L}{2}\begin{cases} - \text{ for } i = a \\ + \text{ for } i = b \end{cases} \tag{C8}$$

A similar result holds for the image terms. By combining the results into an expression for $\tilde{\bar{E}}(\bar{r}_o, \nu)$, the following form is obtained for equation 11:

$$\tilde{\bar{E}}(\bar{r}_o,\nu) \simeq \sqrt{\mu/\epsilon}\,\tilde{f}(\nu)\left\{\frac{e^{jk\rho_c}}{4\pi\rho_c}\,\bar{\epsilon}_R(\rho_c)\sin\left[\tfrac{1}{2}kL(1-\hat{\ell}\cdot\nabla\rho_c)\right] - \right.$$

$$\left. - \frac{e^{jk\rho'_c}}{4\pi\rho'_c}\,\bar{\epsilon}'_R(\rho'_c)\sin\left[\tfrac{1}{2}kL(1-\hat{\ell}'\cdot\nabla\rho'_c)\right]\right\} \tag{C9}$$

where ρ_c' is the distance from the observer to the center of the image filament. Comparison of equation C9 with the solution obtained by making the far-field approximations before integrating (equations 31a and 31b) shows that they are identical. That is, the exact solution and the approximate solution converge to the same result in the fraunhofer region.

APPENDIX D
FREQUENCY DEPENDENCE

APPENDIX D

FREQUENCY DEPENDENCE

This appendix examines the frequency dependence of both the complete and far-field solutions in the special case of an observer on the surface. Because the location of the observer would not be expected to qualitatively effect observations made about frequency dependence and because the solutions are easier to handle than otherwise when the observer is located on the surface, this case has been chosen for analysis.

Consider first the complete solution, and examine the magnitude of the spectrum of the electric field. Then, as shown in equation E8,

$$\sqrt{\tilde{\bar{E}}(\bar{r}_o, \nu) \cdot \tilde{\bar{E}}^*(\bar{r}_o, \nu)} = \sqrt{\mu/\epsilon}\ |\tilde{f}(\nu)|\ \Big\{\ |\alpha|^2 + |\beta|^2 - 2\mathrm{Re}(\alpha\beta^*) \cdot \cos k(L + \rho_b - \rho_a) - 2\,\mathrm{Im}(\alpha\beta^*) \sin k(L + \rho_b - \rho_a)\Big\}^{1/2} \tag{D1}$$

where

$$\alpha = \frac{1}{2\pi\rho_a}\left\{\sqrt{\frac{1 + \hat{\ell} \cdot \nabla\rho_a}{1 - \hat{\ell} \cdot \nabla\rho_a}}\ \hat{\epsilon}(\rho_a) \cdot \hat{z} + j\,\frac{\nabla\rho_a}{k\rho_a}\right\} \tag{D2}$$

$$\beta = \frac{1}{2\pi\rho_b}\left\{\sqrt{\frac{1 + \hat{\ell} \cdot \nabla\rho_b}{1 - \hat{\ell} \cdot \nabla\rho_b}}\ \hat{\epsilon}(\rho_b) \cdot \hat{z} + j\,\frac{\nabla\rho_b}{k\rho_b}\right\} \tag{D3}$$

and where the relationship, $\hat{\ell} \cdot (\bar{r}_b - \bar{r}_a) = L$, has been employed. When the frequency is large enough for the imaginary components of α and β to be negligible,

$$\sqrt{\tilde{\bar{E}}(\bar{r}_o, \nu) \cdot \tilde{\bar{E}}^*(\bar{r}_o, \nu)} \simeq \sqrt{\mu/\epsilon}\ |\tilde{f}(\nu)| \cdot \sqrt{\alpha^2 + \beta^2 - 2\alpha\beta\cos k(L + \rho_b - \rho_a)} \tag{D4}$$

This radical oscillates between the extremes of $|\alpha+\beta|$ and $|\alpha-\beta|$, and, consequently, the mean behavior at large frequencies is determined by $|\tilde{f}(\nu)|$, the magnitude of the spectrum of the current waveform. On the other hand, at low frequencies, the radical in equation D1 is singular because of the $1/k\rho$ dependence of the nonradiation terms, Im α and Im β. This fact is easily seen by rewriting the radical in the following form:

$$\sqrt{\quad} = \Big\{ [(\mathrm{Re}\,\alpha)^2 + (\mathrm{Re}\,\beta)^2 - 2\,(\mathrm{Re}\,\alpha)(\mathrm{Re}\,\beta)\cos k\,(L + \rho_b - \rho_a)] +$$

$$+ [(\mathrm{Im}\,\alpha)^2 + (\mathrm{Im}\,\beta)^2 - 2\,(\mathrm{Im}\,\alpha)(\mathrm{Im}\,\beta)\cos k\,(L + \rho_b - \rho_a)] \qquad \text{(D5)}$$

$$- 2\,\mathrm{Im}\,(\alpha\beta^*)\sin k\,(L + \rho_b - \rho_a) \Big\}^{1/2}$$

In the limit of small k, equation D5 becomes:

$$\sqrt{\quad} \simeq \Big\{ [\,\mathrm{Re}\,\alpha - \mathrm{Re}\,\beta\,]^2 + [\,\mathrm{Im}\,\alpha - \mathrm{Im}\,\beta\,]^2 - \qquad \text{(D6)}$$

$$- 2\,\mathrm{Im}\,(\alpha\beta^*)\sin k\,(L + \rho_b - \rho_a) \Big\}^{1/2}$$

The first and last terms in equation D6 are independent of k, the limit of small k, and the remaining factor, $[\,\mathrm{Im}\,\alpha - \mathrm{Im}\,\beta\,]^2$, depends on $(1/k\rho)^2$. Hence, as $k\rho$ becomes small, the radical becomes large, and the spectrum varies as $|\tilde{f}(\nu)|\,|\mathrm{Im}\,\alpha - \mathrm{Im}\,\beta|$. On the other hand, if only the radiation terms are considered, the radical approaches the constant value, $|\mathrm{Re}\,\alpha - \mathrm{Re}\,\beta|$, for small k. Consequently, the spectrum that is attributable to only the radiation terms varies as $|\tilde{f}(\nu)|$ in both the large and small frequency extremes. At small frequencies, the spectrum attributable to only the radiation components approaches a limit that is proportional to $|\tilde{f}(0)|$, but the spectrum attributable to the complete solution blows up as 1/k because of the singularity in the nonradiation fields at zero frequency.

Next, consider the frequency dependence of the far-field solutions. As shown in equation E11 for the far-field solution observed at the surface,

$$\sqrt{\tilde{\bar{E}}(\bar{r}_o,\nu)\cdot\tilde{\bar{E}}^*(\bar{r}_o,\nu)} = \qquad \text{(D7)}$$

$$\sqrt{\mu/\epsilon}\;\;|\tilde{f}(\nu)|\;\frac{|\hat{\epsilon}(\rho_c)\cdot\hat{z}|}{2\pi\rho_c}\;\Big\{kL\,\mathrm{sinc}\,[\,\tfrac{1}{2}kL(1-\hat{\ell}\cdot\nabla\rho_c)\,]\Big\}$$

For large frequencies, the right-hand side of equation D7 oscillates from a maximum of

$$2\sqrt{\mu/\epsilon}\quad |\tilde{f}(\nu)|\quad \frac{|\hat{\epsilon}(\rho_c)\cdot\hat{z}|}{2\pi\rho_c}\quad [1-\hat{\ell}\cdot\nabla\rho_c]$$

to a minimum of zero. To a first approximation, this is the same as the high-frequency behavior of the complete solution shown in Appendix C. However, at low frequencies, this solution depends on $k\,|\,\tilde{f}(\nu)\,|$, in contrast to the complete solution which appears as $|\tilde{f}(\nu)\,|/k$ if the nonradiation terms are kept or as $|\tilde{f}'(\nu)\,|$ if only the radiation terms are considered. Examples of the spectrum predicted by the far-field solution with the exponential current waveform (Appendix F) were plotted previously in figures 2 through 6. Both the radiation terms of the complete solution and the far-field solution are plotted together for the exponential current waveform. Note the drop in the spectrum as 1/k in the far-field solution at low frequencies and note that both the complete and far-field solutions approximate each other at high frequency.

APPENDIX E
FIELDS ON THE SURFACE

APPENDIX E

FIELDS ON THE SURFACE

When the observer is on the surface (i.e., $z_o = 0$), a symmetry exists at the observation point with respect to the source and image that results in simplification of the solutions. In particular, when $z_o = 0$, the following relationships are obtained for i = a, b:

$$\rho_i = \rho_i' \tag{E1}$$

$$\hat{\ell} \cdot \nabla \rho_i = \hat{\ell}' \cdot \nabla \rho_i' \tag{E2}$$

$$\hat{\ell} \cdot \bar{r}_i = \hat{\ell}' \cdot \bar{r}_i' \tag{E3}$$

and, because

$$\nabla \rho_i' = \nabla \rho_i - 2 (\nabla \rho_i \cdot \hat{z}) \hat{z} \tag{E4}$$

$$\hat{\ell}' = \hat{\ell} - 2 (\hat{\ell} \cdot \hat{z}) \hat{z} \tag{E5}$$

then

$$\hat{\ell} - \hat{\ell}' = 2 (\hat{\ell} \cdot \hat{z}) \hat{z} \tag{E6}$$

$$\nabla \rho_i - \nabla \rho_i' = 2 (\nabla \rho_i \cdot \hat{z}) \hat{z} \tag{E7}$$

By substituting these relationships into equations 11 and 15 of the text, the following forms are obtained for the complete solution as measured by an observer located on the surface:

$$\tilde{\bar{E}} (\bar{r}_o, \nu) = \hat{z} \sqrt{\mu/\epsilon} \; \tilde{f}(\nu) \left\{ \frac{e^{jk\rho_b}}{2\pi\rho_b} \bar{\epsilon}(\rho_b) \cdot \hat{z} - \frac{e^{jk\rho_a}}{2\pi\rho_a} \bar{\epsilon}(\rho_a) \cdot \hat{z} \right\} \tag{E8}$$

$$\tilde{\bar{H}} (\bar{r}_o, \nu) = \tilde{f}(\nu) \left\{ \frac{e^{jk\rho_b}}{2\pi\rho_b} \bar{h}_o(\rho_b) - \frac{e^{jk\rho_a}}{2\pi\rho_a} \bar{h}_o(\rho_a) \right\} \tag{E9}$$

where

$$\bar{h}_o(\rho_i) = e^{jk\hat{\ell}\cdot\bar{r}_i}\sqrt{\frac{1+\hat{\ell}\cdot\nabla\rho_i}{1-\hat{\ell}'\cdot\nabla\rho_i'}}\;\frac{[(\nabla\rho_i\cdot\hat{z})\hat{z}\times\hat{\ell}-(\hat{\ell}\cdot\hat{z})\nabla\rho_i\times\hat{z}]}{\sqrt{1-(\hat{\ell}\cdot\nabla\rho_i)^2}} \tag{E10}$$

Also, substituting the foregoing relationships into equations 31a and 31b of the text, the following form is obtained for the far-field solution as seen by an observer located on the surface:

$$\tilde{\bar{E}}(\bar{r}_o,\nu) = 2j\hat{z}\sqrt{\mu/\epsilon}\;\tilde{f}(\nu)\;\frac{e^{jk\rho_c}}{4\pi\rho_c}\;\bar{\epsilon}_R(\rho_c)\cdot\hat{z}\sin[\tfrac{1}{2}kL(1-\hat{\ell}\cdot\nabla\rho_c)] \tag{E11}$$

$$\tilde{\bar{H}}(\bar{r}_o,\nu) = 2j\tilde{f}(\nu)\;\frac{e^{jk\rho_c}}{4\pi\rho_c}\;\bar{h}_o(\rho_c)\sin[\tfrac{1}{2}kL(1-\hat{\ell}\cdot\nabla\rho_c)] \tag{E12}$$

Note that, in both equations E11 and E12, the electric field intensity is $\hat{z}$-directed and that $h_o(\rho_i)\cdot\hat{z}=0$ for i = a, b, c. Thus, the electric field is perpendicular to the surface, and the magnetic field is tangent to the surface as is required at a perfectly conducting boundary.

APPENDIX F
DISTRIBUTION OF MINIMA FOR THE APPROXIMATE SOLUTION

APPENDIX F

DISTRIBUTION OF MINIMA FOR THE APPROXIMATE SOLUTION

The approximate solution for the i^{th} component of the E field can be written as

$$E_i = (E_i^1 - E_i^2 \tag{F1}$$

$$= K \left\{ \frac{\hat{i} \cdot [\hat{\ell} - (\hat{\ell} \cdot \nabla\rho_c)\nabla\rho_c]}{(\eta - \hat{\ell} \cdot \nabla\rho_c)} \frac{e^{jk(\rho_c + \eta(\hat{\ell} \cdot \bar{r}_c))}}{\rho_c} \sin\frac{kL}{2}(\eta - \hat{\ell} \cdot \nabla\rho_c) \right.$$

$$\left. - \frac{\hat{i} \cdot [\hat{\ell}' - (\hat{\ell}' \cdot \nabla\rho_c')\nabla\rho_c']}{(\eta - \hat{\ell}' \cdot \nabla\rho_c')} \frac{e^{jk(\rho_c' + \eta(\hat{\ell}' \cdot \bar{r}_c'))}}{\rho_c'} \sin\frac{kL}{2}(\eta - \hat{\ell} \cdot \nabla\rho_c') \right\}$$

Zeros of E_i occur when $E_i^1 = E_i^2$, the most important special case of which is $E_i^1 = E_i^2 = 0$, or equivalently,

$$\begin{cases} \tfrac{1}{2}kL(\eta - \hat{\ell} \cdot \nabla\rho_c) = n\pi \\ \tfrac{1}{2}kL(\eta - \hat{\ell}' \cdot \nabla\rho_c') = m\pi \end{cases} \quad n, m \text{ non zero integers} \tag{F2}$$

Equation F2 states that a zero of E_i occurs when the arguments of the sine terms in equation F1 are equal to integer multiples of π. Alternatively, these conditions may be written as

$$\begin{cases} \tfrac{1}{2}kL(\eta - \hat{\ell} \cdot \nabla\rho_c) = n\pi \\ \tfrac{1}{2}kL(\hat{\ell}' \cdot \nabla\rho_c' - \hat{\ell} \cdot \nabla\rho_c) = \ell\pi \end{cases} \quad n, \ell \text{ integers } n \neq 0 \tag{F3}$$

Using $\nu = ck/2\pi$, the frequencies for which $E_i = 0$ are given by

$$\nu = \frac{cn}{L(\eta - \cos\phi)} = \frac{c\ell}{L(\cos\phi' - \cos\phi)}$$

where

$$\cos\phi \equiv \hat{\ell} \cdot \nabla\rho_c$$
$$\cos\phi' \equiv \hat{\ell}' \cdot \nabla\rho_c'$$

The geometrical constraint, implicit in the foregoing equations, is that,

$$\frac{\ell}{n} = \frac{(\cos\phi' - \cos\phi')}{(\eta - \cos\phi)} \tag{F4}$$

To consider the simplest case first, let the observer be located on the perfectly conducting plane, (Z = 0). Then, $\hat{\ell} \cdot \nabla\rho_c = \hat{\ell}' \cdot \nabla\rho_c'$, and conditions of equation F2 are identical (i.e., m = n). The frequency at which E_Z first goes to zero is

$$\nu_1 = \frac{c}{L(\eta - \cos\phi)}$$

Because the zeros are equally spaced, the zero density for a fixed geometry is constant and is given by

$$d = L(\eta - \cos\phi)/c$$

In summary, as L (η - cos φ) increases, the first zero shifts toward lower frequencies and the zero density increases and vice versa. Finally, note that, as $\eta \rightarrow 1$ ($\nu \rightarrow c$), the zero density and first zero become increasingly sensitive to changes in the angle.

For an arbitrary placement of the observer, the analysis is more involved. However, a few qualitative statements can be made:

(a) For an observer above the conducting plane, the probability of satisfying the geometrical constraints imposed by equation F2 is zero. Consequently, the probability of $E_i = 0$, under conditions (i), is zero.

(b) To investigate the minima of E_i, it is helpful to make use of the following definitions:

$$\omega_1 = \omega(\rho_c + \eta(\hat{\ell} \cdot \bar{r}_c))$$

$$\omega_0 = (\omega_1 + \omega_2)/2$$

$$\omega_2 = \omega(\rho_c' + \eta(\hat{\ell}' \cdot \bar{r}_c'))$$

$$\Rightarrow \omega_2 - \omega_0 = \omega_0 - \omega_1 = \Delta\omega\,; \quad \Delta k = \Delta\omega/C$$

Then, $|E_i|$ can be expressed in the form:

$$|E_i| = |\cos \Delta k \left[C_i \sin \frac{kL}{2} (\eta - \cos \phi) - C_i' \sin \frac{kL}{2} (\eta - \cos \phi')\right] -$$

$$- \sin \Delta k \left[C_i \sin \frac{kL}{2} (\eta - \cos \phi) + C_1' \sin \frac{kL}{2} (\eta - \cos \phi')\right] |$$

(c) Special cases:

For $C_i/C_i' >> 1$, $|E_i|$ is minimized at frequencies $\ni \frac{1}{2} kL (\eta - \cos \phi) \approx 2\pi n$.

For $C_i/C_i' << 1$, $|E_i|$ is minimized at frequencies $\ni \frac{1}{2} kL (\eta - \cos \phi') \approx 2\pi m$.

For observation points very close to the conducting plane, $\Delta k << 1$, $C_i/C_i' \approx 1$, strong minima are expected at the frequencies

$$\nu_n = cn/L (\eta - \cos \phi)$$

(d) When none of the foregoing conditions hold, the following procedure seems to give reliable results:

$$\nu_m = cm/L (\eta - \cos \phi')$$

$$\nu_n = cn/L (\eta - \cos \phi)$$

An estimate of the first frequency at which E_i has a well-defined minima is then given by

$$\nu_{c_1} = \frac{C_i}{C_i + C_i'} \nu_{n=1} + \frac{C_i'}{C_i + C_i'} \nu_{m=1}$$

After ν_{c_1} is computed, the density of minima and all subsequent minima can be found. For example, consider the spectrum of the field for the case of a 50-m vertical element as seen by an observer situated at $10^4 (1/\sqrt{2}, 0, 1/\sqrt{2})$ (shown previously in figure 35).

Then,

$$\nu_{c_1} \sim 20.8 \text{ MHz}$$

$$\nu_{c_2} \sim 41.6 \text{ MHz}$$

$$\nu_{c_3} \sim 62.4 \text{ MHz}$$

$$\nu_{c_4} \sim 83.2 \text{ MHz}$$

$$\nu_{c_5} \sim 104 \text{ MHz}$$

These values compare favorably with the values obtained by a high-resolution plot of equation F1 for this case; i.e.,

$$(\nu_{c_1}, \nu_{c_2}, \nu_{c_3}, \nu_{c_4}, \nu_{c_5}) = (21, 42, 61, 81, 102) \text{ MHz}$$

(e) From the preceding discussion, it is evident that the relative magnitudes of C_i, C_i' affect the location of the minima. In general,

$$\left.\begin{array}{l} C_i \doteq C_j \\ C_i' \neq C_j' \end{array}\right\} \quad (i \neq j)$$

Therefore, a possibility exists that the minima of the various field components will occur at significantly different frequencies. Examples of this effect were shown previously in figures 17 and 18.

$$\tilde{\bar{A}}(\bar{r}_o, \nu) = \mu \tilde{f}(\nu) \int_{\text{filament}} e^{j2\pi\nu \left[\frac{\hat{\ell} \cdot \bar{r}'}{v}\right]} \left[\frac{e^{jkR}}{4\pi R} \hat{\ell} - \frac{e^{jkR_I}}{4\pi R_I} \hat{\ell}' \quad d\bar{r}'\right] \tag{18}$$

$$\tilde{\bar{E}}(\bar{r}_o, \nu) = jk\sqrt{\mu/\epsilon}\ \tilde{f}(\nu) \int_{\text{filament}} e^{j2\pi\nu \left[\frac{\ell \cdot \hat{r}'}{v}\right]} \left\{\left[\hat{\ell} + \frac{1}{k^2} (\hat{\ell} \cdot \bar{\nabla}) \nabla\right] \frac{e^{jkR}}{4\pi R} -\right.$$

$$\left. - \left[\hat{\ell}' + \frac{1}{k^2} (\hat{\ell} \cdot \bar{\nabla}) \nabla\right] \frac{e^{jkR_I}}{4\pi R_I}\right\} d\bar{r}' \tag{19}$$

$$R = |\bar{r}_o - \bar{r}'| = |(\bar{r}_o - \bar{r}_c) + (\bar{r}_c - \bar{r}')|$$

$$= \sqrt{|\bar{r}_o - \bar{r}_c|^2 + |\bar{r}_c - \bar{r}'|^2 + 2(\bar{r}_o - \bar{r}_c) \cdot (\bar{r}_c - \bar{r}')}$$

$$\simeq |\bar{r}_o - \bar{r}_c| + |\bar{r}_c - \bar{r}'| \cos\phi + \frac{1}{2} \left[\frac{|\bar{r}_c - \bar{r}'|^2}{|\bar{r}_o - \bar{r}_c|}\right] \tag{20}$$

$$\cos\phi = \frac{(\bar{r}_o - \bar{r}_c) \cdot (\bar{r}_c - \bar{r}')}{|\bar{r}_o - \bar{r}_c|\,|\bar{r}_c - \bar{r}'|} \tag{21}$$

$$kL^2/\rho_c << 1 \tag{22a}$$

$$kL >> 1 \tag{22b}$$

$$\tilde{\bar{E}}(\bar{r}_o, \nu) = jk\sqrt{\mu/\epsilon}\ \tilde{f}(\nu) \left\{\left[\hat{\ell} + \frac{1}{k^2} (\hat{\ell} \cdot \bar{\nabla}) \nabla\right] \frac{e^{jk\rho_c}}{4\pi\rho_c} I(\nu) -\right.$$

$$\left. - \left[\hat{\ell}' + \frac{1}{k^2} (\hat{\ell}' \cdot \bar{\nabla}) \nabla\right] \frac{e^{jk\rho'_c}}{4\pi\rho'_c} I'(\nu)\right\} \tag{23}$$

NASA-Langley, 1976

"The aeronautical and space activities of the United States shall be conducted so as to contribute . . . to the expansion of human knowledge of phenomena in the atmosphere and space. The Administration shall provide for the widest practicable and appropriate dissemination of information concerning its activities and the results thereof."

—NATIONAL AERONAUTICS AND SPACE ACT OF 1958

NASA SCIENTIFIC AND TECHNICAL PUBLICATIONS

TECHNICAL REPORTS: Scientific and technical information considered important, complete, and a lasting contribution to existing knowledge.

TECHNICAL NOTES: Information less broad in scope but nevertheless of importance as a contribution to existing knowledge.

TECHNICAL MEMORANDUMS: Information receiving limited distribution because of preliminary data, security classification, or other reasons. Also includes conference proceedings with either limited or unlimited distribution.

CONTRACTOR REPORTS: Scientific and technical information generated under a NASA contract or grant and considered an important contribution to existing knowledge.

TECHNICAL TRANSLATIONS: Information published in a foreign language considered to merit NASA distribution in English.

SPECIAL PUBLICATIONS: Information derived from or of value to NASA activities. Publications include final reports of major projects, monographs, data compilations, handbooks, sourcebooks, and special bibliographies.

TECHNOLOGY UTILIZATION PUBLICATIONS: Information on technology used by NASA that may be of particular interest in commercial and other non-aerospace applications. Publications include Tech Briefs, Technology Utilization Reports and Technology Surveys.

Details on the availability of these publications may be obtained from:

SCIENTIFIC AND TECHNICAL INFORMATION OFFICE

NATIONAL AERONAUTICS AND SPACE ADMINISTRATION

Washington, D.C. 20546